Available online at www.sciencedirect.com
ScienceDirect
Geochimica et Cosmochimica Acta 72 (2008) 668–689
Geochimica et Cosmochimica Acta
www.elsevier.com/locate/gca

SIMS U–Pb study of zircon from Apollo 14 and 17 breccias: Implications for the evolution of lunar KREEP

A.A. Nemchin [a,*], R.T. Pidgeon [a], M.J. Whitehouse [b], J.P. Vaughan [a], C. Meyer [c]

[a] Curtin University of Technology, Perth, WA 6845, Australia
[b] Swedish Museum of Natural History, S-104 05 Stockholm, Sweden
[c] NASA Johnson Space Center, Houston, TX 77058, United States

Received 13 August 2007; accepted in revised form 9 November 2007; available online 19 November 2007

Abstract

We report the results of a SIMS U–Pb study of 112 zircons from breccia samples from the Apollo 14 and 17 landing sites. Zircon occurs in the breccia matrices as rounded, irregular shaped, broken and rarely euhedral grains and as constituent minerals in a variety of lithic clasts ranging in composition from ultra-mafic and mafic rocks to highly evolved granophyres. Crystallisation of zircon in magmatic rocks is governed by the zirconium saturation in the melt. As a consequence, the presence of zircon in mafic rocks on the Moon implies enrichment of their parent melts in the KREEP component. Our SIMS results show that the ages of zircons from mafic to ultramafic clasts range from ca. 4.35 Ga to ca. 4.00 Ga demonstrating multiple generations of KREEPy mafic and ultramafic magmas over this time period. Individual zircon clasts in breccia matrices have a similar age range to zircons in igneous clasts and all represent zircons that have been incorporated into the breccia from older parents. The age distributions of zircons from breccias from both the Apollo 14 and Apollo 17 landing sites are essentially identical in the range 4.35–4.20 Ga. However, whereas Apollo 14 zircons additionally show ages from 4.20 to 3.90 Ga, no zircons from Apollo 17 samples have primary ages less than ca. 4.20 Ga. Also, in contrast to previous suggestions that the magmatism in the lunar crust is continuous our results show that the zircon age distribution is uneven, with distinct peaks of magmatic activity at ca. 4.35 Ga, ca. 4.20 Ga in Apollo 14 and 17 and a possible third peak in zircons from Apollo 14 at ca. 4.00 Ga. To explain the differences in the zircon age distributions between the Apollo 14 and 17 landing sites we propose that episodes of KREEP magmatism were generated from a primary reservoir, and that this reservoir contracted over time towards the centre of Procellarum KREEP terrane. We attribute the peaks in KREEP magmatism to impact induced emplacement of KREEP magma from a primary mantle source or to a progressive thermal build-up in the mantle source until the temperature exceeds the threshold for generation of KREEP magma, which is transported into the crust by an unspecified possibly plume-like process.

1. INTRODUCTION

One of the most enigmatic features of the geology of the Moon is the presence of high concentrations of large ion lithophile elements in breccias from non-mare regions. This material, referred to as KREEP (Meyer et al., 1971) from its high levels of K, REE and P, also contains relatively high concentrations of other incompatible elements including Th, U and Zr. Fragments of rocks with KREEP trace element signatures have been identified in samples from all Apollo landing sites (Meyer, 1977). Bulk rock chemistry and characteristic Nd isotopic signatures of lunar rocks indicate that KREEP, KREEP basalts, Mg-suite rocks and evolved plutonic rocks, including the alkali suite and a range of siliceous plutonic rocks referred to as granites, have a common petrologic link (James, 1980; Shearer et al., 2006). In addition, enrichment of the incompatible elements in early crystallising phases of Mg-suite rocks

* Corresponding author.
E-mail address: nemchina@kalg.curtin.edu.au (A.A. Nemchin).

0016-7037/$ - see front matter © 2007 Elsevier Ltd. All rights reserved.
doi:10.1016/j.gca.2007.11.009

demonstrates that the KREEP signature of these rocks was characteristic of the parent magma and not a product of late-stage magmatic processes or sub-solidus mixing or mingling (Shearer et al., 2006). From the results of zircon saturation experiments Dickinson and Hess (1982) concluded that only KREEP rich magma has sufficient Zr to produce zircon (i.e. there is an intimate link between the original enrichment of a melt in a KREEP component and the appearance of zircon in rock crystallised from this melt). This association of zircon with enrichment in the incompatible elements observed in Mg-suite rocks, KREEP basalts and evolved rocks, including alkali suite rocks and granites, provides an opportunity to place time constraints on KREEP associated magmatism throughout lunar history.

The advent of high resolution ion microprobes (e.g. Clement and Compston, 1989) has paved the way for precise Secondary Ion Mass Spectrometric (SIMS) U–Pb analyses of lunar zircon (e.g. Compston et al., 1984a,b; Meyer et al., 1996; Pidgeon et al., 2006). U–Pb data on zircons from a variety of lithologies, including granite, alkali gabbro-norite, norite, troctolite and alkali anorthosite have shown that (1) magmatism in the ancient lunar crust extended for more than 400 m.y. rather than being solely the result of a crystallising Lunar Magma Ocean (LMO), (2) individual zircons and zircon-containing rock fragments in the same lunar breccia often have a wide distribution of ages and (3) zircon ages from individual lithologies range from 4.37 to 3.88 Ga (Meyer et al., 1989). The latter is in accord with the conclusion of Nyquist and Shih (1992) that each highland lithology, with the possible exception of the ferroan anorthosites, is characterised by a variety of ages.

The purpose of this study was to further examine and extend the above conclusions and in the following we present the results of an investigation of the morphology and SIMS U–Pb ages of zircons from a number of breccias from Apollo 14 and Apollo 17 landing sites. We discuss the age distributions of zircons from igneous clasts and from the breccia matrices and also for the individual breccias and a combination of breccias representing broadly defined regions within the Apollo 14 and 17 traversed areas. Finally we consider the implications of the combined zircon age distribution patterns from the Apollo 14 and 17 landing sites and propose preliminary models to explain our observations.

2. THE BRECCIA SAMPLES

The location of breccia samples from Apollo 14 and 17 that yielded zircons for the present study are shown in Fig. 1. All investigated Apollo 14 samples, with one exception, have been classified by Simonds et al. (1977) as crystal-

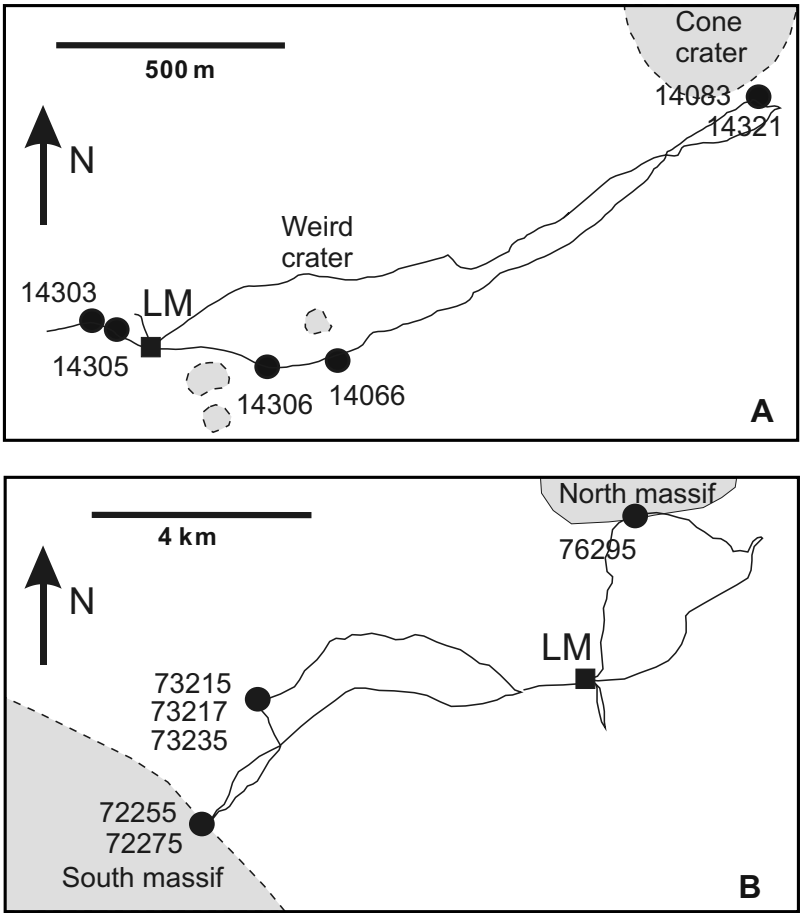

Fig. 1. Apollo 14 and 17 traverses showing sample locations and the areal grouping of samples discussed in the text.

line matrix breccias, implying that the matrices formed as a result of fast crystallisation of an impact melt. Simonds et al. (1977) also described these breccias as belonging to the Fra Mauro type, with over 15% clasts, a number of which are relatively low melting point mineral clasts. This type is also characterised by very few if any glass clasts and <10 μm subhedral to anhedral plagioclase in the matrix, which is often interlocked with pyroxene and minor ilmenite and olivine, forming subophitic to granular textures. Sample 14083 is the only sample that does not show any impact related recrystallisation effects. Simonds et al. (1977) assigned this to their light matrix breccia type, which includes friable, fragmental breccias with a range of clast types and sizes. Stöffler et al. (1979) described these breccias as clastic matrix breccias, implying that they consist of fragments of rocks and minerals with the sizes ranging down to the micron scale. Compared to the set of Apollo 14 sections, our investigated Apollo 17 samples show a much wider textural variation ranging, according to Ryder (1993) and Meyer (1994), from fragmental polymict breccias (sample 72275), through aphanitic impact melt breccias (samples 72255, 73215, 73235), to impact melt breccias (samples 73217 and 76295). This variety demonstrates a transition from breccias that contain very little or no impact melt, to breccias where this melt has recrystallised, to breccias where impact melt has only partly recrystallised or exists as a glass. There are however, discrepancies in the classification of the same samples by different research groups, which suggest that the variation from one type of breccia to another may exist on the scale of individual thin sections of the same sample. For example, in contrast to Meyer (1994) and Ryder (1993), Simonds et al. (1974) described samples 72255 and 72275 as fragmental (clast supported) rocks and sample 73215 as a crystalline matrix breccia with a granular matrix composed of 1–10 μm plagioclase and mafic minerals.

3. RELATIONSHIPS OF THE ZIRCONS TO THEIR HOST BRECCIA

In any breccia, zircon grains occur either within lithic clasts, or as separate mineral clasts in the breccia matrix. Zircons in lithic clasts clearly predate breccia formation. The origin of zircon contained in the matrix is less obvious. There are three possible modes of formation of these zircon grains: (1) they crystallised as cogenetic minerals in plutonic rocks, such as those preserved as lithic clasts, (2) they crystallised from the impact melt during formation of the host breccia or (3) they crystallised from impact melt in older generations of breccias. Textural and size variations between the matrix and the zircon grains provide key information for understanding the processes responsible for zircon formation.

All lunar zircons can be assigned to one of the seven morphological types shown in Fig. 2. Types 1, 2, 3 and 7 are primary zircons that preserve their original morphological features from the time of crystallisation. Types 4, 5 and 6 show features that can be linked to the modification of grains during brecciation or interaction with the impact melt. Two types in the first group are only found in igneous rock clasts. These are the strongly elongated (almost needle like) prismatic grains (Type 1, Fig. 2A) and irregularly shaped zircon growing interstitially with other rock forming minerals (Type 2, Fig. 2B). Type-3 from this group is represented by zircon grains with equally well developed prism and pyramid faces (Fig. 2C). These grains are found in lithic clasts and the matrix. Type-4 grains are represented by zircons that have been fragmented but not abraded during breccia formation. Some of these grains preserve primary features that enable identification of their original morphology. In other grains of this type primary faces have been almost completely removed (Fig. 2D). Most grains of this type are angular fragments with no preserved crystallographic faces (Fig. 2E). Type-5 zircons have smooth subrounded boundaries as a result of mechanical abrasion, and possibly chemical corrosion, during breccia formation (Fig. 2F), whereas Type-6 zircons are mechanically broken grains, strung out as a line of a fragments (e.g. Fig. 2G). Zircons of this type have only been found in igneous rock clasts. Another zircon type (Type-7, shown in Fig. 2H) is a poikilitic, 20–40 μm, impact melt zircon described by Gnos et al. (2004) from lunar meteorite Sayh al Uhaymar 169. The observed texture demonstrates zircon formation during equilibrium crystallisation of the impact melt. The morphology, size and ages of the six zircon types we have identified in lunar breccias demonstrate that they were incorporated into the breccias as separate grains or lithic clasts fragmented from slow cooling plutonic rocks.

4. ANALYTICAL TECHNIQUES

4.1. Preparation of samples

Samples prepared by NASA consisted of polished thin sections of breccias and one polished thin section containing zircon grains from sawdust from a saw-cut through breccia 14321. We did not attempt to add a standard zircon to these mounts but used an external standard for reducing the SIMS data. Sawdust samples from breccias 72255 and 72275 were processed at Curtin University using magnetic and heavy liquid (methylene iodide) separation techniques and recovered zircons were mounted in epoxy discs, together with chips of zircon standard CZ3. Samples were gold coated and U and Pb isotopes were measured using the SHRIMP II at Curtin University of Technology (Perth, Western Australia) and the CAMECA IMS1270 ion microprobe at the Museum of Natural History in Stockholm (Sweden).

4.2. IMS 1270 analyses

The SIMS methodology used at the Nordsim facility closely follows previously published analytical descriptions (Whitehouse et al., 1999; Whitehouse and Kamber, 2005). A molecular oxygen beam (O_2^-) at −13 kV was imaged through an aperture, giving a ca. 6 nA current in an elliptical, ca. 20 μm spot. Secondary ions were extracted from the sample at +10 kV and admitted, via high magnification transfer optics, to the mass spectrometer operating at a mass resolution ($M/\Delta M$) of 5300. Oxygen flooding of the

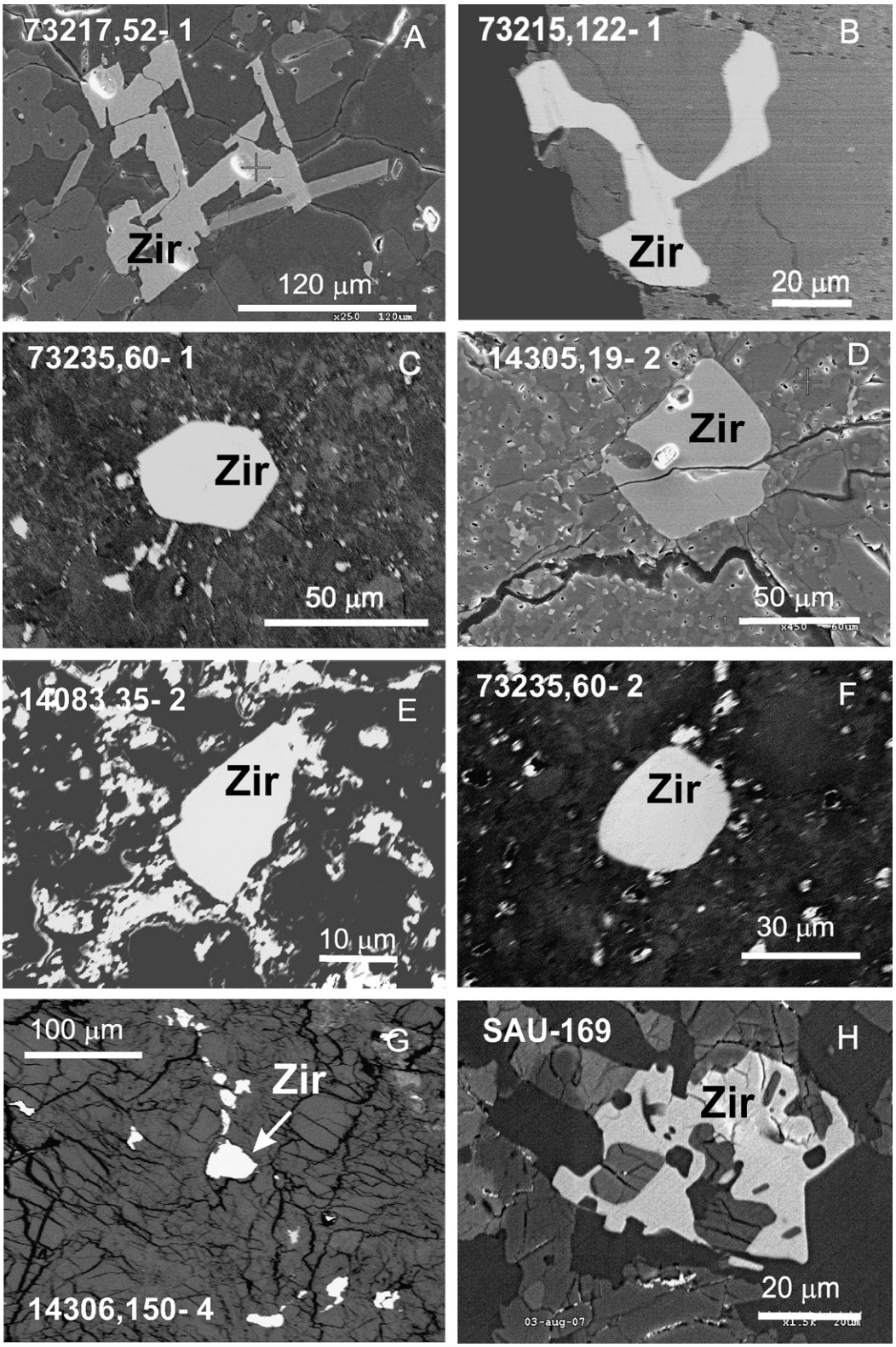

Fig. 2. Shows backscattered electron images of seven morphological zircon types recognised in lunar breccias: (A) elongated prismatic zircon (Type-1); (B) irregularly shaped zircon growing at the boundary of plagioclase grains (Type-2); (C) euhedral zircon with equal development of prism and pyramid faces (Type-3); (D) fragmented grain with some of the original faces preserved (Type-4); (E) fragmented angular grain with none of the original faces visible (Type-4); (F) zircon rounded as a result of abrasion (Type-5); (G) multiple zircon fragments (Type-6); (H) poikilitic impact melt zircon from the sample SAU169 (Type-7), image obtained in the Museum of Natural History in Stockholm with the permission of Edwin Gnos.

sample chamber was used to enhance Pb^+ yield. At the start of each analysis, a 2 min pre-sputter raster over 25 μm was used to remove the Au coating to minimise surface contamination. This was followed by automated centring of the beam in the field aperture, optimisation of mass calibration using selected high-intensity peaks of the mono-collection routine and optimisation of secondary ion energy in the 60 eV energy window. The peak-hopping data collection routine consisted of 16 cycles through the mass stations, with signals measured on an ion counting electron multiplier with a 44 ns electronically gated dead time. Pb/U ratios were calibrated using an empirical correlation between Pb^+/U^+ and UO_2^+/U^+ ratios, normalised to the 1065 Ma Geostandards 91500 zircon (Wiedenbeck et al., 2004).

4.3. SHRIMP-II analyses

The SHRIMP methodology follows analytical procedure described by Compston et al. (1984a) and Kennedy and de Laeter (1994). The filtered (O_2^-) beam with intensity between 3 and 4 nA was focused to ca. 20 μm spot on the surface of the zircon samples. Secondary ions were passed to the mass spectrometer operating at a mass resolution ($M/\Delta M$) of ~5000. Each analysis was preceded by a 3 min rastering to remove the Au coating. The peak-hopping data collection routine consisted of seven scans through the mass stations, with signals measured on an ion counting electron multiplier. Pb/U ratios were calibrated using an empirical correlation between Pb^+/U^+ and UO^+/U^+ ratios, normalised to the 564 Ma Sri-Lankan zircon CZ3 (Pidgeon et al., 1994). The 1.5–1.8% error obtained from the multiple analyses of the Pb/U ratio of the standard during individual SHRIMP sessions was added in quadrature to the errors observed in the unknowns. The initial data reduction was done using SQUID AddIn for Microsoft Excel (Ludwig, 2001a) and Isoplot (Ludwig, 2001b) was used for age calculations.

4.4. Initial Pb correction

The initial Pb correction of lunar samples is complicated by the highly radiogenic Pb compositions of many lunar rocks (e.g.Gale, 1972; Tera and Wasserburg, 1972), which suggest a substantial early loss of Pb from the Moon. Meyer et al. (1996) argued that a systematic change of $^{206}Pb/^{204}Pb$ during SHRIMP analyses of lunar zircon suggests surface contamination as a result of smearing of Pb from the surrounding sample over the zircon surface during polishing. Consequently they used a model where the initial Pb selected for the correction was calculated as a mixture of meteoritic Pb (assumed to be similar to Canyon Diablo troilite Pb) and radiogenic lunar Pb (determined by Compston et al., 1991 in feldspars from the felsic clasts found in lunar breccias). The mixing equations were solved in the $^{208}Pb/^{206}Pb$ vs. $^{204}Pb/^{206}Pb$ coordinate system by calculating radiogenic $^{208}Pb/^{206}Pb$ from the measured Th/U and the approximate age followed by finding the intersection of a line determined by joining the calculated radiogenic $^{208}Pb/^{206}Pb$ at zero $^{204}Pb/^{206}Pb$ and the point defined by the measured $^{208}Pb/^{206}Pb$ vs. $^{204}Pb/^{206}Pb$ of the zircon and the mixing line between Canyon Diablo troilite Pb and lunar feldspar Pb.

When a similar approach is applied to the zircon grains investigated in the present study a significant number of analyses are so close to the abscissa that the correction calculations are within the uncertainties and most analyses do not intersect the mixing line. However, four sections in the analysed set appear to contain most of the grains with high $^{204}Pb/^{206}Pb$ confirming the conclusion of Meyer et al. (1996) that contaminant Pb is the result of surface contamination. The trend determined by these analyses in the $^{208}Pb/^{206}Pb$ vs. $^{204}Pb/^{206}Pb$ coordinate system (Fig. 3) points towards modern terrestrial model Pb (Stacey and Kramers, 1975), suggesting that the sample surface is contaminated by terrestrial Pb, or a fortuitous mixing composition of Canyon Diablo and lunar feldspar Pb defined by the intersection of the trend and the mixing line. Our conclusion is that surface contamination on the NASA polished thin sections is from common Pb introduced during the polishing and we have corrected all zircon analyses using the Stacey–Kramers model, modern, common Pb compositions. We have found no cases where this correction is demonstrably incorrect.

4.5. Bias in the calculated $^{206}Pb/^{238}U$

A consequence of the necessity to use an external standard to calculate elemental ratios for ion probe analysis of zircons in the NASA thin sections is that this limits the accuracy of U/Pb ratios, resulting in a slight reverse discordance of data (about 2%). This is illustrated on Fig. 4A which shows that a large proportion of analytical points, with Pb/U calculated using an external CZ3 standard, are slightly reversely discordant when plotted on a concordia diagram. However, this discordance is not present in analyses of zircons from the two sawdust samples of Apollo-17 breccias, where the Curtin CZ3 standard has been added to the mount and is situated close to the sawdust zircon grains.

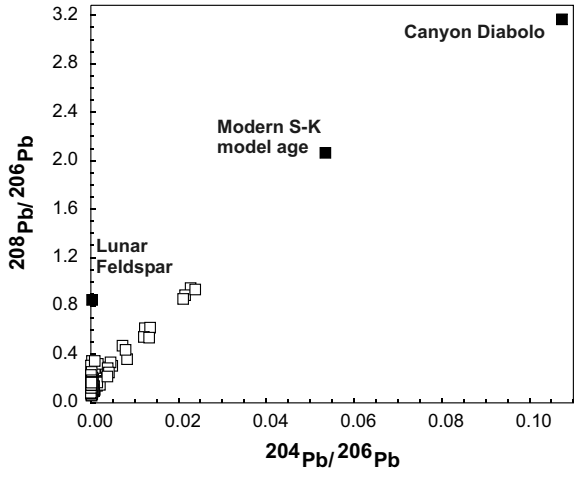

Fig. 3. Distribution of measured $^{208}Pb/^{206}Pb$ versus $^{204}Pb/^{206}Pb$ for the lunar zircons. Analyses with significant initial Pb are seen to approximate a line trending to modern Pb.

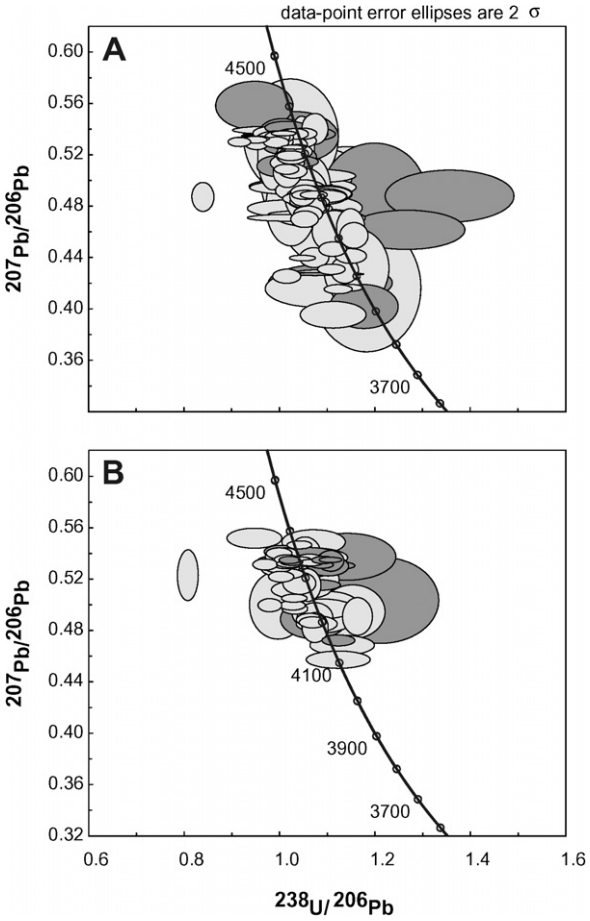

Fig. 4. Tera Wasserburg concordia plots of corrected zircon analyses of samples from Apollo 14 (A) and Apollo 17 (B). Light grey: analyses with external standard; Dark grey: analyses with standard and lunar zircons on the same mount.

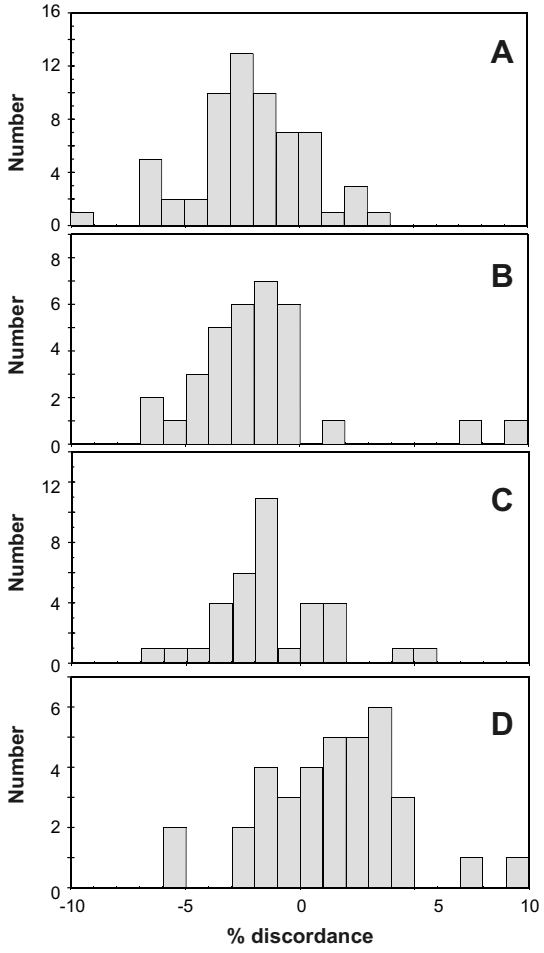

Fig. 5. Histograms of % discordance obtained for U–Pb analyses of: (A) zircon grains in the Apollo 14 thin sections; (B) zircon grains in the Apollo 17 thin sections; (C) zircon grains from the sawdust of Apollo 14 sample 14321; (D) zircon grains from the sawdust of Apollo 17 samples 72255 and 72275.

The concordia plots also clearly illustrate the age limits of the lunar samples with all analyses, although slightly reversely discordant on Fig. 4A, falling close to concordia between the outer age limits (including 2σ uncertainties) of 3800 Ma and 4450 Ma. The bias in the $^{206}Pb/^{238}U$ ages is also shown on histogram plots in Fig. 5. Approximately 80% of analytical points for the zircon in thin sections, where the standard was analysed in a separate mount, have negative values for per cent discordance with maximums on the histograms at about −2% (Fig. 5A–C), suggesting an overall reverse discordance. The histogram in Fig. 5D shows that analyses of zircons from two Apollo 17 sawdust samples mounted with the standard have essentially zero per cent discordance. The consistency of the bias suggests that a blanket correction of −2% to the external standard derived $^{206}Pb/^{238}U$ data in Tables 1 and 2 would result in a better estimate of the true values of the ratios.

5. THE ANALYTICAL RESULTS

SIMS analytical results of 112 zircons from eleven thin sections, analysed using the IMS1270 instrument in Stockholm and six samples including three sawdust concentrates, analysed using the SHRIMP II ion microprobe in Perth are listed in Tables 1 (Apollo 14) and 2 (Apollo 17) where analyses are grouped according to locations of breccias in the traversed areas (Fig. 1). Data are shown on a concordia plot in Fig. 4. All errors for individual ratios and ages are 1-sigma unless specified.

Allowing for the approximately 2% bias in the $^{206}Pb/^{238}U$ measurements it is evident from Fig. 4 that most analyses are concordant. In this paper we are concerned with the distribution of primary zircon ages and whereas it could be assumed that concordant ages signify undisturbed zircon U–Pb systems, previous experience has shown (e.g. Pidgeon et al., 2007) that the ages of analytical spots on isotopically disturbed lunar zircons are generally concordant but can also be inconsistent indicating a disturbed U–Pb system. Consequently we have made multiple SIMS analyses of many of the zircon grains (Tables 1 and 2) to test for age consistency in an apparently homogeneous grain and to explore the U–Pb systematics of grains that are suspected of having a history of isotopic disturbance. Where repeat analyses are consistent within the uncertainty, the age is interpreted as the primary crystallisation age of

Table 1
Ion probe U–Pb results for the zircon grains from the Apollo 14 samples

Spot[a]	Type[b]	Size (μm)	Occurrence	U (ppm)	Th (ppm)	^{206}Pb (ppm)	$\frac{Th}{U}$	$\frac{^{206}Pb}{^{204}Pb}$	% err[c]	$\frac{^{207}Pb}{^{206}Pb}$	$\frac{^{208}Pb}{^{206}Pb}$	$\frac{^{238}U}{^{206}Pb}$	$\frac{^{208}Pb}{^{232}Th}$	% comPb[d]	$\frac{^{238}U}{^{206}Pb^*}$	$\frac{^{207}Pb^{*5}}{^{206}Pb^*}$	% disc[e]	$\frac{^{207}Pb^*}{^{206}Pb^*}$ Age (Ma)	$\frac{^{206}Pb^*}{^{238}U}$ Age (Ma)
Western part of the traverse																			
Sample 14303																			
Section 49																			
1-1	1	700 × 200	Felsic clast	74	27	120	0.37	724	4	0.5417 ± 16	0.140 ± 2	0.978 ± 11	0.393 ± 15	2.58	1.004 ± 11	0.5339 ± 16	−3	4338 ± 4	4457 ± 49
1-2				74	24	116	0.33	11710	14	0.5201 ± 16	0.085 ± 1	1.023 ± 12	0.251 ± 10	0.16	1.024 ± 12	0.5196 ± 16	−2	4298 ± 4	4392 ± 50
2-1	6	80 × 20	Felsic clast	149	64	237	0.43	863	19	0.5258 ± 22	0.160 ± 7	1.005 ± 12	0.371 ± 21	2.17	1.027 ± 13	0.5189 ± 26	−2	4296 ± 7	4382 ± 54
2-2				199	135	345	0.68	739	5	0.5376 ± 17	0.240 ± 1	0.969 ± 11	0.363 ± 13	2.53	0.994 ± 11	0.5299 ± 17	-4	4327 ± 5	4487 ± 49
3-1	1	270 × 20	Felsic clast	541	319	878	0.59	15806	7	0.5266 ± 7	0.151 ± 1	1.030 ± 11	0.248 ± 9	0.12	1.031 ± 11	0.5262 ± 7	−1	4316 ± 2	4370 ± 46
4-1	6	240 × 80	Felsic clast	574	350	968	0.61	12441	8	0.5373 ± 8	0.166 ± 1	1.008 ± 11	0.272 ± 10	0.15	1.009 ± 11	0.5369 ± 8	−2	4346 ± 2	4439 ± 47
Section 52																			
1-1	4	50 × 45	Small Px-aggregate	41	27	64	0.68	3408	19	0.4279 ± 22	0.179 ± 2	1.011 ± 12	0.264 ± 10	0.55	1.016 ± 12	0.4257 ± 23	−10	4002 ± 8	4416 ± 52
2-1	4	35 × 25	Matrix	305	418	600	1.38	4089	6	0.5343 ± 8	0.346 ± 1	0.948 ± 11	0.268 ± 10	0.46	0.952 ± 11	0.5329 ± 9	−7	4335 ± 2	4627 ± 55
3-1	3	230 × 180	Ol-Px clast	67	50	102	0.74	81	10	0.5615 ± 113	0.617 ± 44	0.847 ± 22	0.989 ± 83	23.02	1.100 ± 41	0.4795 ± 184	0	4179 ± 56	4169 ± 157
3-2				62	47	102	0.77	5668	16	0.5259 ± 104	0.203 ± 2	1.044 ± 11	0.256 ± 10	0.33	1.048 ± 11	0.5249 ± 104	0	4313 ± 29	4319 ± 45
3-3				61	29	84	0.49	206	5	0.4973 ± 54	0.305 ± 7	1.046 ± 11	0.606 ± 26	9.10	1.150 ± 12	0.4634 ± 62	2	4129 ± 20	4033 ± 42
4-1	5	55 × 35	Attached to Pl grain	46	26	74	0.57	44	5	0.6628 ± 81	0.947 ± 47	0.589 ± 14	2.866 ± 187	42.55	1.025 ± 41	0.5348 ± 182	−1	4340 ± 49	4388 ± 174
5-1	3	130 × 60	Matrix	164	111	253	0.68	4248	10	0.4906 ± 12	0.179 ± 1	1.068 ± 11	0.248 ± 9	0.44	1.073 ± 12	0.4891 ± 12	−1	4209 ± 4	4245 ± 46
5-2				134	93	211	0.70	305	10	0.5094 ± 21	0.288 ± 11	0.985 ± 11	0.419 ± 22	6.14	1.049 ± 11	0.4880 ± 31	−3	4205 ± 9	4316 ± 45
6-1	5	140 × 50	Matrix	47	23	73	0.50	1816	8	0.5258 ± 23	0.136 ± 1	1.030 ± 12	0.269 ± 10	1.03	1.041 ± 12	0.5226 ± 23	−1	4306 ± 7	4341 ± 49
6-2				68	33	112	0.48	2320	9	0.5327 ± 21	0.133 ± 1	0.994 ± 11	0.280 ± 10	0.81	1.002 ± 11	0.5303 ± 21	−3	4328 ± 6	4461 ± 50
6-3				76	41	124	0.54	1817	7	0.5390 ± 18	0.153 ± 1	1.015 ± 12	0.279 ± 10	1.03	1.026 ± 13	0.5359 ± 18	−1	4343 ± 5	4387 ± 54
7-1	4	50 × 35	Matrix	44	24	70	0.55	5506	15	0.5287 ± 24	0.141 ± 1	1.027 ± 12	0.249 ± 9	0.34	1.031 ± 12	0.5277 ± 24	−1	4320 ± 7	4371 ± 50
8-1	2	70 × 35	Small Pl-Px clast	88	59	136	0.67	293	4	0.4934 ± 23	0.293 ± 4	0.986 ± 11	0.444 ± 17	6.39	1.054 ± 12	0.4701 ± 26	−4	4150 ± 8	4302 ± 48
9-1	3	60 × 25	Matrix	76	54	108	0.71	223	6	0.4892 ± 32	0.335 ± 12	1.060 ± 12	0.448 ± 22	8.38	1.157 ± 12	0.4575 ± 41	2	4110 ± 13	4015 ± 42
10-1	4	45 × 20	Matrix	69	28	114	0.41	47	3	0.6459 ± 44	0.889 ± 30	0.590 ± 9	3.762 ± 198	40.17	0.986 ± 12	0.5185 ± 105	−5	4295 ± 29	4515 ± 56
11-1	4	30 × 30	Matrix	61	16	89	0.26	121	9	0.5423 ± 53	0.361 ± 24	0.894 ± 12	1.547 ± 119	15.47	1.058 ± 19	0.4887 ± 85	−2	4207 ± 26	4290 ± 75
Sample 14305																			
Section 19																			
1-1	4	45 × 35	Matrix	1457	1639	2859	1.13	633	11	0.5391 ± 10	0.322 ± 4	0.890 ± 9	0.321 ± 12	2.95	0.917 ± 10	0.5301 ± 14	−10	4327 ± 4	4753 ± 50
2-1	4	70 × 55	Matrix	107	87	183	0.82	138	6	0.5520 ± 36	0.472 ± 17	0.880 ± 9	0.659 ± 34	13.51	1.018 ± 12	0.5076 ± 52	−3	4264 ± 15	4412 ± 53
3-1	4	105 × 90	Matrix	60	36	94	0.60	74	3	0.6150 ± 27	0.621 ± 15	0.804 ± 9	1.295 ± 58	25.26	1.075 ± 11	0.5404 ± 49	3	4355 ± 13	4239 ± 44
4-1	3	80 × 40	Matrix	43	22	55	0.53	83	12	0.5115 ± 114	0.545 ± 45	0.916 ± 25	1.131 ± 105	22.62	1.184 ± 46	0.4167 ± 204	1	3970 ± 71	3948 ± 155
4-2				124	76	173	0.61	792	6	0.4400 ± 41	0.200 ± 2	1.111 ± 12	0.297 ± 11	2.36	1.138 ± 12	0.4305 ± 42	−1	4019 ± 14	4066 ± 42
5-1	3	55 × 35	Matrix	36	12	56	0.34	1852	11	0.5172 ± 27	0.104 ± 1	1.007 ± 15	0.303 ± 13	1.01	1.018 ± 15	0.5140 ± 27	−3	4282 ± 8	4412 ± 64
6-1	3	90 × 55	In a Pl grain	51	16	71	0.32	42	2	0.6446 ± 53	0.936 ± 11	0.597 ± 6	4.879 ± 190	44.50	1.076 ± 13	0.4914 ± 107	0	4216 ± 32	4236 ± 52
6-2				88	28	138	0.32	1142	9	0.5247 ± 45	0.107 ± 2	1.006 ± 11	0.337 ± 14	1.64	1.023 ± 11	0.5195 ± 46	−2	4298 ± 13	4396 ± 48
Central part of the traverse																			
Sample 14306																			
Section 60																			
1-1	3	400 × 300	Norite clast	39	22	32	0.58	904	15	0.4909 ± 17	0.181 ± 5	1.042 ± 16	0.292 ± 0	2.07	1.064 ± 17	0.4836 ± 20	−2	4192 ± 6	4270 ± 68
2-1	1	400 × 50	Norite clast	26	16	20	0.62	2020	21	0.4931 ± 21	0.176 ± 2	1.094 ± 19	0.255 ± 5	0.93	1.105 ± 19	0.4899 ± 23	1	4211 ± 7	4156 ± 72

3-1	3	250 × 130	Norite clast	44	30	35	0.69	1972	31	0.4911 ± 16	0.194 ± 3	1.089 ± 17	0.252 ± 5	0.95	1.100 ± 17	0.4878 ± 19	1	4205 ± 6	4169 ± 65
4-1	4	100 × 60	Norite clast	29	17	25	0.60	261	12	0.5119 ± 20	0.287 ± 14	0.989 ± 17	0.470 ± 25	7.16	1.066 ± 21	0.4869 ± 38	−2	4202 ± 12	4266 ± 83
5-1	4	125 × 50	Norite clast	11	4	11	0.35	75	14	0.5695 ± 69	0.539 ± 50	0.860 ± 20	1.752 ± 168	24.85	1.145 ± 62	0.4814 ± 185	3	4185 ± 57	4047 ± 218
6-1	4	100 × 60	Norite clast	33	16	27	0.47	6712	52	0.4872 ± 19	0.127 ± 1	1.047 ± 17	0.249 ± 5	0.28	1.050 ± 17	0.4862 ± 020	−3	4200 ± 6	4312 ± 72
7-1	3	100 × 70	Norite clast	33	20	27	0.59	1108	24	0.4937 ± 20	0.172 ± 2	1.078 ± 18	0.263 ± 5	1.69	1.096 ± 19	0.4878 ± 25	1	4205 ± 7	4180 ± 73
Section 150																			
1-1	3	60 × 35	Matrix	73	42	116	0.58	20193	20	0.5368 ± 18	0.152 ± 1	1.051 ± 12	0.255 ± 10	0.09	1.052 ± 12	0.5366 ± 18	1	4345 ± 5	4308 ± 47
1-2				76	43	124	0.57	25322	22	0.5368 ± 17	0.151 ± 1	1.033 ± 11	0.265 ± 10	0.07	1.034 ± 11	0.5365 ± 17	0	4345 ± 5	4361 ± 48
2-1	4	100 × 40	Matrix	83	45	140	0.55	5564	10	0.5350 ± 18	0.143 ± 1	0.994 ± 11	0.264 ± 10	0.34	0.997 ± 11	0.5339 ± 18	−3	4338 ± 5	4478 ± 49
2-2				41	13	63	0.33	1601	9	0.5347 ± 22	0.112 ± 2	1.031 ± 14	0.328 ± 14	1.17	1.044 ± 14	0.5311 ± 23	0	4330 ± 6	4332 ± 60
3-1	4	30 × 25	Matrix	154	85	270	0.55	40514	17	0.5322 ± 11	0.140 ± 1	0.950 ± 10	0.266 ± 10	0.05	0.951 ± 10	0.5321 ± 11	−7	4333 ± 3	4633 ± 49
4-1	6	65 × 50	Norite clast	151	57	209	0.38	26618	16	0.4472 ± 23	0.097 ± 1	1.112 ± 12	0.230 ± 9	0.07	1.112 ± 12	0.4469 ± 23	−1	4075 ± 8	4134 ± 44
4-2		30 × 20		154	49	205	0.32	13356	13	0.4162 ± 14	0.088 ± 1	1.122 ± 12	0.243 ± 9	0.14	1.124 ± 12	0.4156 ± 15	−3	3967 ± 5	4103 ± 44
4-3		50 × 20		121	70	166	0.58	10658	12	0.4176 ± 12	0.152 ± 1	1.138 ± 15	0.230 ± 9	0.18	1.140 ± 15	0.4168 ± 12	−2	3971 ± 4	4060 ± 53
4-4		25 × 15		78	60	121	0.78	9201	13	0.4816 ± 32	0.194 ± 1	1.069 ± 12	0.232 ± 9	0.20	1.071 ± 12	0.4809 ± 32	−2	4184 ± 10	4251 ± 46
4-5		25 × 15		137	82	220	0.60	3935	27	0.4822 ± 127	0.176 ± 5	1.021 ± 22	0.289 ± 17	0.48	1.025 ± 22	0.4805 ± 128	−5	4183 ± 39	4388 ± 93
Sample 14066																			
Section 47																			
1-1	4	110 × 50	Matrix	25	11	22	0.44	490	10	0.4922 ± 23	0.149 ± 2	0.984 ± 35	0.340 ± 13	3.82	1.023 ± 36	0.4786 ± 28	−5	4177 ± 9	4396 ± 156
2-1	5	50 × 30	Matrix	123	62	107	0.51	10578	28	0.5397 ± 13	0.137 ± 1	0.984 ± 34	0.264 ± 9	0.18	0.986 ± 34	0.5392 ± 13	−4	4352 ± 3	4516 ± 154
3-1	5	100 × 60	Matrix	39	13	32	0.31	1965	18	0.4981 ± 28	0.094 ± 1	1.060 ± 37	0.262 ± 10	0.95	1.070 ± 37	0.4948 ± 29	−1	4226 ± 9	4253 ± 147
4-1	5	60 × 40	Matrix	126	50	102	0.40	5569	27	0.4750 ± 11	0.113 ± 1	1.063 ± 36	0.258 ± 10	0.34	1.067 ± 36	0.4738 ± 12	−2	4162 ± 4	4263 ± 146
5-1	4	70 × 30	Matrix	271	152	231	0.57	2109	16	0.4744 ± 9	0.161 ± 2	1.010 ± 34	0.275 ± 10	0.89	1.019 ± 35	0.4711 ± 11	−6	4153 ± 3	4409 ± 150
Eastern part of the traverse																			
Sample 14083																			
Section 35																			
1-1	4	50 × 20	Matrix	57	35	104	0.61	6646	16	0.5303 ± 21	0.203 ± 6	0.950 ± 10	0.352 ± 16	0.28	0.953 ± 10	0.5294 ± 21	−7	4325 ± 6	4626 ± 51
2-1	4	25 × 15	Matrix	225	260	375	1.16	24740	14	0.4401 ± 9	0.308 ± 1	1.048 ± 11	0.254 ± 9	0.08	1.049 ± 11	0.4398 ± 9	−7	4051 ± 3	4316 ± 46
3-1	4	25 × 20	Matrix	30	15	41	0.50	9701	21	0.4423 ± 23	0.130 ± 2	1.148 ± 14	0.228 ± 9	0.19	1.151 ± 14	0.4415 ± 24	1	4057 ± 8	4032 ± 47
4-1	5	15 × 15	Matrix	75	36	113	0.48	11997	15	0.4748 ± 26	0.128 ± 1	1.059 ± 12	0.254 ± 10	0.16	1.061 ± 12	0.4742 ± 26	−3	4163 ± 8	4280 ± 50
5-1	5	15 × 15	Matrix	28	24	61	0.86	1134	26	0.4931 ± 42	0.346 ± 7	0.827 ± 9	0.478 ± 22	1.65	0.841 ± 9	0.4874 ± 46	−20	4204 ± 14	5052 ± 56
6-1	4	40 × 25	Matrix	207	79	321	0.39	100052	28	0.5075 ± 23	0.092 ± 1	1.029 ± 12	0.232 ± 9	0.02	1.029 ± 12	0.5075 ± 23	−3	4263 ± 7	4375 ± 50
6-2				241	98	381	0.41	333717	38	0.5088 ± 16	0.098 ± 1	1.015 ± 11	0.234 ± 9	*0.01	1.015 ± 11	0.5088 ± 16	−4	4267 ± 5	4419 ± 46
7-1	4	130 × 90	Attached to Pl	101	62	157	0.62	103873	35	0.4892 ± 15	0.148 ± 1	1.055 ± 12	0.226 ± 9	0.02	1.055 ± 12	0.4892 ± 15	−2	4209 ± 4	4298 ± 47
7-2				43	14	64	0.33	15427	24	0.4917 ± 21	0.082 ± 1	1.052 ± 12	0.234 ± 9	0.12	1.053 ± 12	0.4913 ± 21	−2	4215 ± 6	4303 ± 49
Sample 14321																			
Section 16																			
1-1	3	30 × 15	Anorthosite clast	87	48	130	0.55	127	2	0.4988 ± 23	0.437 ± 6	0.915 ± 11	0.861 ± 35	14.78	1.074 ± 12	0.4403 ± 32	−5	4053 ± 11	4243 ± 49
2-1	4	40 × 40	Anorthosite clast	79	41	102	0.53	48	3	0.5909 ± 53	0.858 ± 22	0.705 ± 12	2.321 ± 109	39.33	1.162 ± 28	0.4322 ± 125	1	4025 ± 42	4003 ± 96
2-2				130	45	179	0.35	1804	9	0.4353 ± 16	0.112 ± 1	1.098 ± 12	0.302 ± 12	1.04	1.109 ± 12	0.4311 ± 16	−3	4021 ± 6	4142 ± 45
14321 sawdust																			
2-1				8	3	6	0.36	6501	99	0.4216 ± 60	0.108 ± 7	1.105 ± 53	0.262 ± 16	0.29	1.108 ± 53	0.4204 ± 61	−4	3984 ± 22	4146 ± 199
2-2				7	3	6	0.36	2414	61	0.4194 ± 56	0.107 ± 7	1.071 ± 44	0.268 ± 15	0.77	1.080 ± 44	0.4161 ± 59	−6	3968 ± 21	4225 ± 173
1-1				808	333	639	0.41	71729	28	0.4275 ± 5	0.111 ± 1	1.087 ± 37	0.239 ± 8	0.03	1.087 ± 37	0.4274 ± 5	−5	4008 ± 2	4205 ± 143
20-1				30	10	25	0.34	6237	56	0.5371 ± 27	0.089 ± 3	1.026 ± 36	0.248 ± 10	0.30	1.029 ± 37	0.5362 ± 27	−1	4344 ± 7	4376 ± 155
20-2				32	12	28	0.37	4018	41	0.5376 ± 27	0.101 ± 3	1.010 ± 36	0.264 ± 11	0.47	1.015 ± 36	0.5362 ± 28	−2	4344 ± 8	4422 ± 157
20-3				33	11	28	0.35	28624	38	0.5258 ± 24	0.088 ± 2	1.016 ± 19	0.181 ± 7	0.05	1.015 ± 19	0.5261 ± 24	−2	4316 ± 7	4420 ± 84
20-4				33	12	28	0.36	66725	80	0.5370 ± 24	0.092 ± 2	0.991 ± 19	0.188 ± 7	0.02	0.991 ± 19	0.5369 ± 24	−3	4346 ± 7	4497 ± 85
12-1				225	104	192	0.47	18332	49	0.5342 ± 11	0.122 ± 1	1.008 ± 34	0.252 ± 9	0.10	1.009 ± 34	0.5339 ± 11	−2	4338 ± 3	4440 ± 152

(*continued on next page*)

Table 1 (*continued*)

Spot[a]	Type[b]	Size (μm)	Occurrence	U (ppm)	Th (ppm)	^{206}Pb (ppm)	Th/U	$\frac{^{206}Pb}{^{204}Pb}$	% err[c]	$\frac{^{207}Pb}{^{206}Pb}$	$\frac{^{208}Pb}{^{206}Pb}$	$\frac{^{238}U}{^{206}Pb}$	$\frac{^{208}Pb}{^{232}Th}$	% comPb[d]	$\frac{^{238}U}{^{206}Pb^*}$	$\frac{^{207}Pb^{*5}}{^{206}Pb^*}$	% disc[e]	$\frac{^{207}Pb^*}{^{206}Pb^*}$ Age (Ma)	$\frac{^{206}Pb^*}{^{238}U}$ Age (Ma)
12-2				263	127	224	0.49	16354	18	0.5353 ± 10	0.129 ± 1	1.006 ± 35	0.255 ± 9	0.11	1.007 ± 35	0.5350 ± 10	−2	4341 ± 3	4446 ± 154
11-1				52	28	42	0.54	6336	41	0.5048 ± 22	0.142 ± 3	1.066 ± 37	0.240 ± 9	0.30	1.069 ± 37	0.5038 ± 22	0	4252 ± 6	4257 ± 149
11-2				31	18	25	0.59	4045	45	0.5022 ± 28	0.156 ± 5	1.055 ± 38	0.243 ± 9	0.46	1.060 ± 38	0.5006 ± 29	−1	4243 ± 9	4284 ± 153
10-1				51	29	43	0.57	3873	25	0.4972 ± 22	0.149 ± 4	1.020 ± 36	0.249 ± 9	0.48	1.025 ± 36	0.4956 ± 22	−4	4228 ± 7	4388 ± 154
10-2				53	29	45	0.55	3452	22	0.4964 ± 21	0.150 ± 3	1.021 ± 36	0.261 ± 10	0.54	1.026 ± 36	0.4946 ± 21	−4	4225 ± 6	4385 ± 153
8-1				15	6	9	0.42	1786	41	0.4917 ± 80	0.120 ± 10	1.344 ± 54	0.207 ± 12	1.05	1.358 ± 55	0.4880 ± 83	15	4205 ± 25	3558 ± 145
8-2				16	5	11	0.32	1323	32	0.4670 ± 59	0.098 ± 7	1.251 ± 49	0.238 ± 013	1.41	1.268 ± 50	0.4617 ± 62	9	4123 ± 20	3747 ± 146
13-1				61	26	55	0.43	8366	29	0.5592 ± 76	0.115 ± 4	0.946 ± 33	0.272 ± 10	0.22	0.948 ± 33	0.5586 ± 77	−5	4404 ± 20	4642 ± 161
13-2				64	30	53	0.46	13701	40	0.5335 ± 81	0.123 ± 3	1.035 ± 37	0.251 ± 9	0.14	1.034 ± 37	0.5339 ± 81	−1	4338 ± 22	4362 ± 156
14-1				88	31	70	0.36	12017	24	0.4796 ± 39	0.096 ± 2	1.082 ± 37	0.240 ± 9	0.16	1.083 ± 37	0.4791 ± 39	−1	4178 ± 12	4215 ± 146
14-2				82	29	65	0.35	6460	55	0.4721 ± 29	0.095 ± 2	1.086 ± 38	0.239 ± 9	0.29	1.089 ± 38	0.4710 ± 29	−1	4153 ± 9	4200 ± 145
14-3				89	33	68	0.38	27257	24	0.4607 ± 67	0.096 ± 2	1.116 ± 19	0.163 ± 6	0.05	1.117 ± 19	0.4604 ± 67	0	4119 ± 22	4122 ± 71
21-1				50	26	41	0.53	51452	74	0.5149 ± 19	0.135 ± 2	1.036 ± 19	0.177 ± 6	0.03	1.036 ± 19	0.5148 ± 19	−2	4284 ± 5	4356 ± 80
21-2				51	27	44	0.54	179139	371	0.5114 ± 33	0.132 ± 2	0.999 ± 18	0.177 ± 6	0.01	0.999 ± 18	0.5113 ± 33	−5	4274 ± 10	4472 ± 83
21-3				78	43	65	0.55	45383	74	0.5189 ± 32	0.141 ± 2	1.034 ± 18	0.178 ± 6	0.03	1.034 ± 18	0.5187 ± 32	−2	4295 ± 9	4360 ± 76
24-1				12	4	10	0.33	2241	46	0.3998 ± 38	0.098 ± 6	1.107 ± 28	0.193 ± 10	0.62	1.114 ± 28	0.3957 ± 42	−6	3893 ± 16	4130 ± 104
24-2				13	4	9	0.33	9203	102	0.4031 ± 69	0.093 ± 5	1.176 ± 29	0.172 ± 8	0.15	1.178 ± 29	0.4021 ± 70	−1	3917 ± 26	3962 ± 99
100-1				80	49	67	0.62	84495	115	0.5332 ± 27	0.163 ± 3	1.023 ± 18	0.185 ± 7	0.02	1.023 ± 18	0.5331 ± 27	−1	4336 ± 8	4395 ± 79
100-2				83	53	71	0.64	19319	33	0.5336 ± 22	0.160 ± 2	0.997 ± 18	0.182 ± 7	0.07	0.997 ± 18	0.5333 ± 22	−3	4336 ± 6	4477 ± 80
100-3				42	22	36	0.52	27180	68	0.5375 ± 25	0.135 ± 3	1.008 ± 20	0.185 ± 8	0.05	1.008 ± 20	0.5377 ± 25	−2	4348 ± 7	4443 ± 90
25-1				19	6	16	0.34	28683	110	0.5017 ± 151	0.085 ± 4	1.023 ± 25	0.178 ± 8	0.05	1.023 ± 25	0.5014 ± 151	−4	4245 ± 44	4394 ± 108
25-2				19	7	14	0.39	18919	80	0.4911 ± 157	0.113 ± 4	1.198 ± 44	0.174 ± 9	0.07	1.199 ± 44	0.4907 ± 158	7	4213 ± 47	3909 ± 144
22-1				60	38	51	0.65	14467	43	0.5387 ± 42	0.163 ± 4	1.006 ± 19	0.181 ± 7	0.10	1.007 ± 19	0.5381 ± 42	−2	4349 ± 12	4447 ± 84
22-2				55	35	46	0.65	11452	29	0.5419 ± 21	0.163 ± 2	1.015 ± 18	0.179 ± 6	0.12	1.016 ± 19	0.5412 ± 21	−1	4358 ± 6	4417 ± 81
23-1				23	8	19	0.37	43537	287	0.4925 ± 35	0.103 ± 4	1.046 ± 22	0.192 ± 8	0.03	1.047 ± 22	0.4923 ± 36	−2	4218 ± 11	4323 ± 92
23-2				38	20	30	0.54	36330	174	0.4900 ± 27	0.137 ± 3	1.101 ± 21	0.171 ± 6	0.04	1.101 ± 21	0.4898 ± 27	1	4211 ± 8	4164 ± 81

[a] Grain and spot number.
[b] Morphological type of zircon.
[c] 1 sigma % error.
[d] Proportion of common ^{206}Pb.
[e] Per cent discordance.

Table 2
Ion probe U–Pb results for the zircon grains from the Apollo 17 samples

Spot[a]	Type[b]	Size (μm)	Occurrence	U (ppm)	Th (ppm)	^{206}Pb (ppm)	Th/U	$\frac{^{206}Pb}{^{204}Pb}$	% err[c]	$\frac{^{207}Pb}{^{206}Pb}$	$\frac{^{208}Pb}{^{206}Pb}$	$\frac{^{238}U}{^{206}Pb}$	$\frac{^{208}Pb}{^{232}Th}$	% comPb[d]	$\frac{^{238}U}{^{206}Pb^*}$	$\frac{^{207}Pb^{*5}}{^{206}Pb^*}$	% disc[e]	$\frac{^{207}Pb^*}{^{206}Pb^*}$ Age (Ma)	$\frac{^{206}Pb^*}{^{238}U}$ Age (Ma)
Station 2																			
Sample 72255																			
72255 sawdust																			
2-1				13	7	11	0.53	15973	76	0.4858 ± 25	0.140 ± 2	1.078 ± 17	0.239 ± 5	0.12	1.079 ± 18	0.4854 ± 25	−1	4197 ± 8	4228 ± 50
4-1				31	16	24	0.52	4006	25	0.4742 ± 17	0.144 ± 2	1.119 ± 14	0.242 ± 5	0.47	1.124 ± 14	0.4725 ± 17	1	4158 ± 5	4102 ± 38
5-1				92	31	77	0.34	222956	99	0.5334 ± 10	0.089 ± 1	1.026 ± 10	0.247 ± 3	0.01	1.026 ± 10	0.5334 ± 10	−1	4336 ± 3	4386 ± 30
6-1				119	62	100	0.52	180647	87	0.5351 ± 12	0.133 ± 1	1.022 ± 9	0.244 ± 3	0.01	1.023 ± 9	0.5351 ± 12	−1	4341 ± 3	4397 ± 29
8-1				25	8	21	0.32	11914	46	0.5419 ± 21	0.081 ± 1	1.001 ± 14	0.249 ± 5	0.16	1.003 ± 14	0.5414 ± 21	−2	4358 ± 6	4459 ± 44
9-1				69	31	55	0.46	6248	38	0.5377 ± 27	0.127 ± 2	1.082 ± 23	0.248 ± 7	0.30	1.085 ± 24	0.5368 ± 27	3	4346 ± 7	4209 ± 67
11-1				92	41	76	0.45	691	59	0.4987 ± 24	0.168 ± 18	1.044 ± 22	0.351 ± 43	2.71	1.073 ± 29	0.4893 ± 63	−1	4209 ± 19	4245 ± 84
12-1				52	26	42	0.51	4300	32	0.5210 ± 52	0.139 ± 2	1.058 ± 25	0.253 ± 7	0.43	1.063 ± 26	0.5197 ± 53	1	4298 ± 15	4275 ± 75
13-1				34	12	28	0.34	1616	20	0.5525 ± 38	0.106 ± 2	1.060 ± 27	0.286 ± 9	1.16	1.072 ± 27	0.5492 ± 39	3	4379 ± 10	4248 ± 78
14-1				235	184	182	0.79	16136	42	0.5312 ± 15	0.216 ± 1	1.105 ± 21	0.241 ± 5	0.12	1.107 ± 21	0.5309 ± 15	4	4329 ± 4	4150 ± 59
15-1				193	181	158	0.94	5180	18	0.5259 ± 15	0.256 ± 1	1.047 ± 20	0.252 ± 5	0.36	1.051 ± 20	0.5248 ± 15	0	4312 ± 4	4311 ± 61
16-1				188	85	151	0.46	6519	18	0.5347 ± 16	0.125 ± 1	1.071 ± 20	0.249 ± 5	0.29	1.074 ± 21	0.5338 ± 16	2	4337 ± 4	4241 ± 59
17-1				60	27	48	0.45	1987	18	0.5405 ± 26	0.131 ± 2	1.068 ± 24	0.263 ± 7	0.94	1.078 ± 25	0.5377 ± 26	3	4348 ± 7	4230 ± 71
19-1				76	28	61	0.37	6227	26	0.5338 ± 22	0.101 ± 2	1.079 ± 23	0.249 ± 7	0.30	1.083 ± 23	0.5329 ± 22	3	4335 ± 6	4217 ± 66
20-1				20	7	16	0.35	243	16	0.5607 ± 058	0.251 ± 10	1.055 ± 35	0.662 ± 36	7.71	1.143 ± 42	0.5377 ± 75	7	4348 ± 20	4053 ± 109
21-1				82	17	67	0.21	6764	38	0.5344 ± 30	0.060 ± 1	1.039 ± 22	0.268 ± 8	0.28	1.041 ± 22	0.5336 ± 30	0	4337 ± 8	4339 ± 67
22-1				102	24	82	0.24	3158	27	0.5369 ± 23	0.074 ± 1	1.070 ± 22	0.280 ± 7	0.59	1.076 ± 22	0.5351 ± 23	2	4341 ± 6	4236 ± 64
23-1				164	121	139	0.74	2763	14	0.5360 ± 15	0.209 ± 2	1.013 ± 20	0.269 ± 6	0.68	1.020 ± 20	0.5339 ± 15	−2	4338 ± 4	4405 ± 62
Sample 72275																			
72275 sawdust																			
1-1				94	39	76	0.42	1461	15	0.5197 ± 17	0.134 ± 1	1.062 ± 21	0.295 ± 7	1.28	1.075 ± 22	0.5156 ± 18	1	4286 ± 5	4238 ± 62
2-1				56	28	45	0.50	2922	20	0.5346 ± 22	0.141 ± 2	1.079 ± 23	0.257 ± 7	0.64	1.086 ± 23	0.5326 ± 22	3	4334 ± 6	4208 ± 66
3-1				78	39	68	0.50	2237	25	0.5367 ± 17	0.147 ± 2	0.996 ± 20	0.288 ± 7	0.84	1.00 ± 20	0.5342 ± 19	−3	4339 ± 5	4453 ± 65
4-1				31	14	28	0.45	1432	18	0.5558 ± 31	0.139 ± 3	0.936 ± 23	0.321 ± 11	1.31	0.948 ± 24	0.5521 ± 32	−5	4387 ± 8	4642 ± 83
6-1				89	30	72	0.34	1919	15	0.5376 ± 30	0.111 ± 1	1.054 ± 21	0.305 ± 7	0.97	1.065 ± 21	0.5347 ± 31	2	4340 ± 9	4270 ± 62
7-1				96	52	78	0.54	3322	26	0.5423 ± 16	0.153 ± 1	1.054 ± 21	0.261 ± 6	0.56	1.060 ± 21	0.5407 ± 17	2	4356 ± 5	4284 ± 62
9-1				251	83	213	0.33	6382	32	0.5359 ± 16	0.091 ± 2	1.014 ± 19	0.265 ± 7	0.29	1.017 ± 19	0.5351 ± 17	−2	4341 ± 5	4416 ± 59
12-1				90	55	71	0.61	251197	99	0.5314 ± 11	0.156 ± 1	1.088 ± 10	0.228 ± 2	0.01	1.089 ± 10	0.5314 ± 11	3	4331 ± 3	4201 ± 29
13-1				41	4	35	0.10	7699	48	0.5007 ± 108	0.065 ± 8	0.995 ± 24	0.624 ± 94	0.24	0.998 ± 25	0.4999 ± 108	−5	4241 ± 32	4475 ± 79
14-1				15	9	12	0.60	2078	24	0.5330 ± 30	0.166 ± 2	1.093 ± 17	0.248 ± 5	0.90	1.102 ± 18	0.5302 ± 31	4	4328 ± 9	4162 ± 49
15-1				59	34	48	0.59	33053	64	0.5471 ± 13	0.151 ± 1	1.042 ± 11	0.241 ± 3	0.06	1.043 ± 11	0.5469 ± 13	1	4373 ± 3	4335 ± 32
16-1				64	32	50	0.50	5667	21	0.5354 ± 33	0.13 ± 1	1.104 ± 11	0.231 ± 3	0.33	1.108 ± 11	0.5344 ± 33	5	4339 ± 9	4147 ± 31
17-1				10	4	8	0.40	266	49	0.5272 ± 56	0.217 ± 40	1.129 ± 19	0.468 ± 87	7.03	1.214 ± 49	0.5038 ± 137	10	4252 ± 40	3874 ± 119
20-1				74	39	61	0.53	179237	42	0.5349 ± 11	0.137 ± 1	1.044 ± 10	0.241 ± 3	−0.02	1.043 ± 10	0.5350 ± 11	0	4341 ± 3	4333 ± 30
21-1				85	32	68	0.38	28640	42	0.5333 ± 10	0.099 ± 1	1.066 ± 10	0.236 ± 3	0.07	1.067 ± 10	0.5331 ± 10	2	4335 ± 3	4263 ± 29
22-1				27	16	21	0.62	22364	67	0.5345 ± 18	0.159 ± 1	1.070 ± 13	0.23 ± 4	0.08	1.071 ± 13	0.5343 ± 18	2	4339 ± 5	4251 ± 39
25-1				237	166	186	0.70	66304	26	0.5351 ± 11	0.179 ± 1	1.092 ± 10	0.227 ± 2	0.03	1.092 ± 10	0.5350 ± 11	4	4341 ± 3	4191 ± 28

(*continued on next page*)

Table 2 (*continued*)

Spot[a]	Type[b]	Size (μm)	Occurrence	U (ppm)	Th (ppm)	^{206}Pb (ppm)	Th/U	$\frac{^{206}Pb}{^{204}Pb}$	% err[c]	$\frac{^{207}Pb}{^{206}Pb}$	$\frac{^{208}Pb}{^{206}Pb}$	$\frac{^{238}U}{^{206}Pb}$	$\frac{^{208}Pb}{^{232}Th}$	% comPb[d]	$\frac{^{238}U}{^{206}Pb^*}$	$\frac{^{207}Pb^{*5}}{^{206}Pb^*}$	% disc[e]	$\frac{^{207}Pb^*}{^{206}Pb^*}$ Age (Ma)	$\frac{^{206}Pb^*}{^{238}U}$ Age (Ma)
26-1				123	66	96	0.54	71494	47	0.5353 ± 9	0.137 ± 1	1.107 ± 10	0.223 ± 2	0.03	1.108 ± 10	0.5352 ± 9	5	4341 ± 2	4147 ± 27
Station 3																			
Sample 73215																			
Section 122																			
1-1	2	130 × 20	Small Pl aggregate	65	27	107	0.42	9519	14	0.538 ± 26	0.108 ± 1	0.995 ± 11	0.257 ± 10	0.20	0.997 ± 11	0.5381 ± 26	−3	4349 ± 7	4477 ± 50
1-2				68	28	110	0.42	34324	27	0.5292 ± 18	0.107 ± 1	1.012 ± 12	0.253 ± 10	0.05	1.012 ± 12	0.5290 ± 18	−2	4324 ± 5	4428 ± 54
1-3				71	27	117	0.38	6169	11	0.5315 ± 30	0.100 ± 1	0.986 ± 11	0.269 ± 10	0.30	0.989 ± 11	0.5305 ± 30	−4	4328 ± 8	4505 ± 52
2-1	3	30 × 15	Matrix	199	79	310	0.40	31243	16	0.4999 ± 15	0.100 ± 1	1.027 ± 11	0.245 ± 9	0.06	1.028 ± 11	0.499 ± 15	−3	4240 ± 4	4380 ± 47
2-2				213	88	330	0.41	9169	8	0.4977 ± 16	0.107 ± 1	1.030 ± 11	0.255 ± 9	0.20	1.032 ± 11	0.4970 ± 16	−3	4232 ± 5	4367 ± 47
3-1	5	30 × 20	Matrix	69	25	101	0.37	277940	68	0.4825 ± 48	0.089 ± 1	1.075 ± 11	0.229 ± 9	0.01	1.075 ± 11	0.4825 ± 48	−1	4189 ± 15	4238 ± 44
3-2				53	17	72	0.33	68534	45	0.4913 ± 060	0.083 ± 1	1.163 ± 13	0.225 ± 9	0.03	1.164 ± 13	0.4912 ± 60	5	4215 ± 18	3998 ± 44
Sample 73217																			
Section 52																			
1-1	2	100 × 30	Small Pl-Px aggreagte	252	216	444	0.87	30550	17	0.5001 ± 21	0.230 ± 1	0.980 ± 10	0.273 ± 10	0.06	0.981 ± 10	0.4999 ± 21	−7	4241 ± 6	4532 ± 48
1-2				185	116	390	0.63	4403	7	0.5246 ± 80	0.186 ± 7	0.805 ± 9	0.375 ± 24	0.42	0.809 ± 9	0.5232 ± 80	−20	4308 ± 22	5190 ± 58
2-1	1	160 × 30	Small Pl-Px aggreagte	166	82	269	0.50	47669	22	0.5321 ± 12	0.12 ± 1	1.021 ± 11	0.245 ± 9	0.04	1.021 ± 11	0.5319 ± 12	−2	4332 ± 3	4401 ± 47
2-2				169	90	277	0.53	79700	27	0.5314 ± 13	0.135 ± 1	1.016 ± 11	0.250 ± 9	0.02	1.017 ± 11	0.5313 ± 13	−2	4331 ± 3	4415 ± 49
Sample 73235																			
Section 54																			
1-1	4	35 × 25	Matrix	36	12	56	0.33	5772	17	0.5180 ± 35	0.089 ± 1	1.039 ± 14	0.265 ± 11	0.32	1.042 ± 14	0.5170 ± 35	−1	4290 ± 10	4336 ± 58
2-1	4	25 × 20	Matrix	91	26	145	0.29	25346	19	0.5293 ± 15	0.076 ± 1	0.997 ± 11	0.263 ± 11	0.07	0.998 ± 11	0.5291 ± 15	−3	4324 ± 4	4475 ± 51
3-1	4	220 × 180	Matrix	63	36	104	0.58	19968	25	0.5365 ± 23	0.145 ± 1	1.012 ± 11	0.250 ± 9	0.09	1.013 ± 11	0.5362 ± 23	−2	4344 ± 6	4426 ± 49
3-2				64	37	107	0.58	33756	31	0.5403 ± 18	0.146 ± 1	0.999 ± 11	0.253 ± 10	0.06	1.000 ± 11	0.5402 ± 18	−3	4355 ± 5	4469 ± 50
4-1	5	35 × 30	Matrix	69	27	117	0.39	6353	15	0.5326 ± 18	0.105 ± 1	0.968 ± 11	0.280 ± 11	0.29	0.971 ± 11	0.5317 ± 18	−5	4332 ± 5	4565 ± 51
5-1	5	30 × 25	Matrix	41	14	62	0.34	14502	26	0.5160 ± 52	0.102 ± 1	1.059 ± 11	0.293 ± 12	0.13	1.060 ± 11	0.515 ± 52	0	4287 ± 15	4283 ± 46
Section 60																			
1-1	5	20 × 15	Matrix	173	92	272	0.53	207894	50	0.5357 ± 17	0.132 ± 1	1.064 ± 12	0.239 ± 9	0.01	1.064 ± 12	0.5357 ± 17	2	4342 ± 5	4272 ± 48
2-1	5	40 × 30	Matrix	140	77	230	0.56	72658	41	0.5221 ± 17	0.130 ± 1	1.003 ± 11	0.230 ± 9	0.03	1.004 ± 011	0.5220 ± 17	−4	4305 ± 5	4456 ± 48
2-2				124	65	203	0.53	68263	30	0.5374 ± 30	0.120 ± 1	1.015 ± 11	0.222 ± 8	0.03	1.016 ± 11	0.5374 ± 30	−2	4347 ± 8	4418 ± 48
3-1	4	80 × 35	In a Pl grain	85	28	124	0.33	25279	26	0.4869 ± 18	0.079 ± 1	1.069 ± 12	0.224 ± 9	0.07	1.070 ± 12	0.4867 ± 18	−1	4201 ± 5	4254 ± 46
3-2				82	29	121	0.36	70935	41	0.4888 ± 20	0.084 ± 1	1.065 ± 12	0.216 ± 8	0.03	1.065 ± 12	0.4887 ± 20	−1	4207 ± 6	4268 ± 48
4-1	3	55 × 45	Matrix	107	67	179	0.63	53511	29	0.5397 ± 20	0.147 ± 1	1.014 ± 11	0.230 ± 9	0.03	1.014 ± 11	0.5396 ± 20	−2	4353 ± 6	4424 ± 48
Section 80																			
1-1	5	45 × 30	Attached to a Px grain	10	5	15	0.53	2592	27	0.4929 ± 46	0.143 ± 3	1.067 ± 15	0.254 ± 12	0.72	1.075 ± 15	0.4904 ± 47	−1	4213 ± 14	4240 ± 60
1-2				10	5	16	0.51	5916	33	0.5374 ± 67	0.134 ± 3	1.050 ± 15	0.258 ± 12	0.32	1.054 ± 15	0.5364 ± 68	1	4345 ± 18	4303 ± 61
2-1	5	90 × 90	Matrix	98	57	162	0.59	37190	23	0.5342 ± 19	0.14 ± 1	1.010 ± 11	0.244 ± 9	0.05	1.010 ± 11	0.5341 ± 19	−2	4338 ± 5	4436 ± 49
2-2				94	56	155	0.60	57498	35	0.5356 ± 15	0.149 ± 1	1.016 ± 11	0.246 ± 9	0.03	1.016 ± 11	0.5355 ± 15	−2	4342 ± 4	4416 ± 47

Station 6																			
Sample 76295																			
Section 91																			
1-1	4	90 × 30	Small Pl-Px aggreagte	129	69	204	0.54	43335	23	0.5056 ± 13	0.127 ± 1	1.031 ± 11	0.228 ± 9	0.04	1.032 ± 11	0.5055 ± 13	−3	4257 ± 4	4369 ± 47
1-2				88	46	143	0.53	30034	21	0.5245 ± 15	0.124 ± 1	1.020 ± 13	0.229 ± 9	0.06	1.020 ± 13	0.5243 ± 15	−2	4311 ± 4	4404 ± 54
2-1	4	260 × 100	Matrix	55	33	42	0.61	16401	61	0.4579 ± 27	0.161 ± 2	1.122 ± 27	0.228 ± 6	0.11	1.124 ± 27	0.4575 ± 27	0	4110 ± 9	4103 ± 100
2-2				54	30	44	0.57	6527	18	0.5129 ± 30	0.145 ± 2	1.043 ± 26	0.240 ± 7	0.29	1.046 ± 26	0.5120 ± 30	−1	4276 ± 9	4325 ± 106
2-3				40	23	31	0.58	105068	50	0.5002 ± 40	0.153 ± 2	1.100 ± 28	0.234 ± 7	0.02	1.098 ± 28	0.5008 ± 40	2	4243 ± 12	4175 ± 106
2-4				52	34	40	0.66	10381	51	0.4695 ± 32	0.173 ± 2	1.130 ± 27	0.226 ± 6	0.18	1.132 ± 27	0.4688 ± 32	2	4146 ± 10	4081 ± 99
2-5				60	39	47	0.64	17261	20	0.4975 ± 31	0.166 ± 2	1.091 ± 26	0.230 ± 6	0.11	1.092 ± 26	0.4971 ± 31	1	4233 ± 9	4191 ± 100
2-6				40	23	31	0.58	15763	59	0.4945 ± 62	0.148 ± 2	1.094 ± 28	0.229 ± 7	0.12	1.096 ± 28	0.4941 ± 63	1	4224 ± 19	4180 ± 108
2-7				55	35	41	0.64	8768	10	0.4956 ± 86	0.168 ± 2	1.152 ± 28	0.223 ± 6	0.21	1.154 ± 28	0.4948 ± 86	5	4226 ± 26	4023 ± 96

[a] Grain and spot number.
[b] Morphological type of zircon.
[c] 1 sigma % error.
[d] Proportion of common ^{206}Pb.
[e] Per cent discordance.

the parent igneous rock. For example three analyses of zircon in a plagioclase rich clast in thin section 73215,122 gave $^{207}Pb/^{206}Pb$ ages of 4349 ± 7 Ma, 4324 ± 5 Ma and 4328 ± 8 Ma, which are indistinguishable within the uncertainties and the average age is interpreted as the best estimate of the age of crystallisation of the parent rock. There are, however, a number of examples in the data set of zircons with U–Pb systems that have been disturbed, probably in response to extreme heat generated during a major impact. The best studied of these is the complex zircon aggregate in an anorthositic clast in section 73235,82 (Smith et al., 1986; Pidgeon et al., 2007). These authors reported two ages for this complex zircon, which they interpreted as recording the age of primary crystallisation of the parent anorthosite at 4315 ± 15 Ma, and the age of restructuring and complete Pb loss of the zircon during an impact at 4187 ± 11 Ma. Complex zircon ages provide a window into a deeper understanding of lunar processes and we are currently continuing our investigation into these zircons. However where the interpretation of the ages of some complex grains is uncertain we have omitted the data from consideration in this paper.

6. THE DISTRIBUTION OF ZIRCON AGES IN MAFIC IGNEOUS CLASTS

In the studied samples the zircons are found in lithic clasts of a few millimetres or less than a millimetre in size, making it difficult to define the host rock precisely according to the igneous rock classification. Nevertheless, relatively large clasts containing 10–20 individual crystals of one or more minerals are referred to by the rock name defined from the mineral composition. Where the clast consists of a few crystals we refer to it, for example, as a "pyroxene" or "pyroxene-plagioclase" aggregate.

Meyer et al. (1989) concluded, on the basis of a SIMS U–Pb study of zircons in a variety of igneous clasts, including granite, alkali gabbro-norite, norite, troctolite and alkali anorthosite, that zircons in any one rock type can have a range of ages from 4.37 to 3.88 Ga. This was well demonstrated by Meyer et al. (1996) for lunar granites, which they showed to have a wide range of ages from 4.32 to 3.88 Ga. The large age range of Mg- and alkali suite rocks from ca. 4.4 to 3.9 Ga has also been described by Nyquist and Shih (1992). Snyder et al. (2000) and Shearer et al. (2006) concluded that these data indicate initiation of Mg-suite magmatism soon after the formation of the primitive ferroan anorthosite crust and magmatic history that extended for 100 s of millions of years. SIMS analyses reported in Tables 1 and 2 on zircons included in rock clasts several mm in size provide a further test for the above conclusions (Fig. 6). These clasts include two norite (thin sections 14306,60 and 14306,150), one anorthosite (thin section 14321,16) and one olivine–pyroxene rich fragment (thin section 14303,52). Zircon grains have also been identified in six less than 1 mm plagioclase, pyroxene and plagioclase –pyroxene fragments (grains 1 and 8 in the section 14303,52; grain 1 in the section 73215,122; grains 1 and 2 in the section 73217,52 and grain 1 in the section 76295,91). In addition, five analysed zircons are attached to or included in the plagioclase

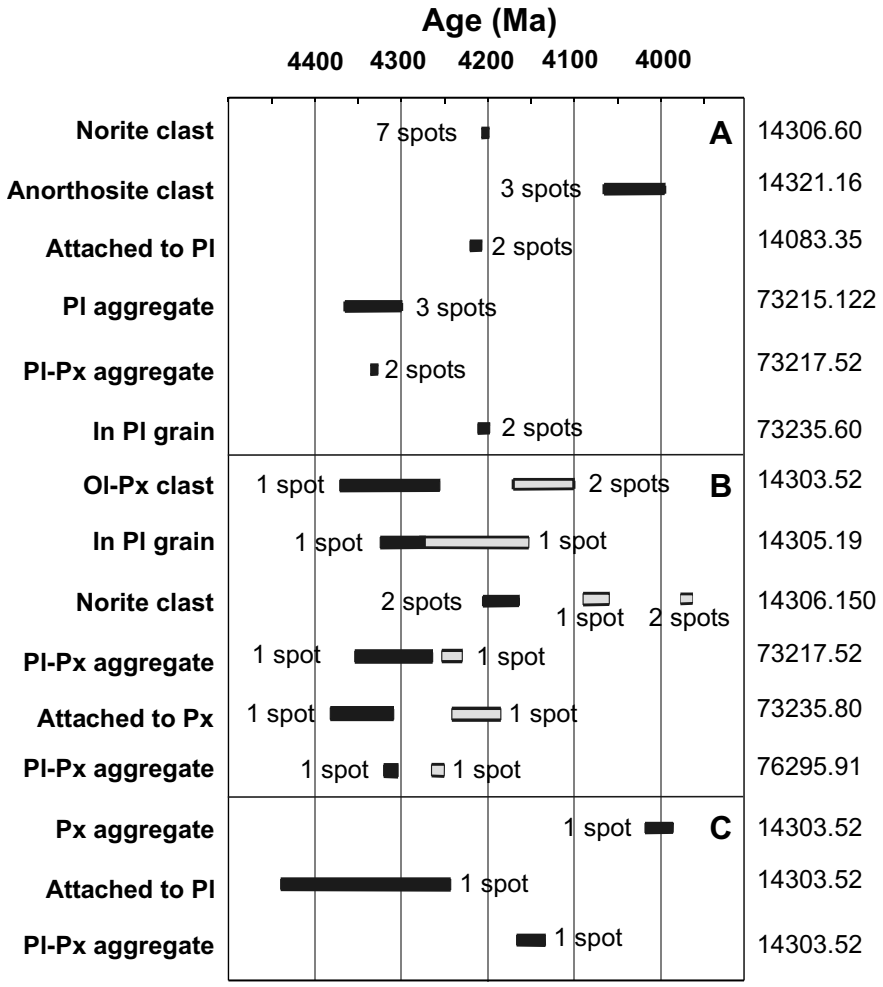

Fig. 6. Distribution of $^{207}Pb/^{206}Pb$ ages of zircon bearing lithic clasts from Apollo 14 and Apollo 17 breccias (box lengths are 2-sigma).

or pyroxene mineral clasts (grain 4 in the section 14303,52; grain 6 in the section 14305,19; grain 7 in the section 14083,35; grain 3 in the section 73235,60 and grain 1 in the section 73235,80). Most of these rock and mineral fragments are consistent with a norite composition. The anorthosite and olivine–pyroxene rich clasts may represent differentiates of basaltic magma that formed norites or belong to an entirely different suite of plutonic rocks. Nevertheless, these clasts (with the exception of one felsic clast from sample 14303) represent a suite of mafic and ultramafic rocks, in contrast to the granite clasts described by Meyer et al. (1996).

These mafic clasts contain either a single zircon large enough to accommodate several SIMS analyses or several smaller zircon crystals large enough for a single analysis. Four large zircon grains and two groups of smaller zircons show internally consistent ages determined from multiple analyses (Fig. 6A). The average of these ages is interpreted as the age of formation of the plutonic rocks represented by these clasts. Although rocks represented by these clasts may belong to the same chemical suite, it is clear from Fig. 6A that their ages extend from 4.35 to 4.00 Ga and it is also seen that they fall into three different age groups with peaks at ca. 4.33, ca. 4.21 and ca. 4.03 Ga.

Six clasts contain zircon grains that show a variation of ages outside the analytical errors (Fig. 6B). Additional work will be required to fully understand the resetting of U–Pb systems in these zircons. However, the oldest ages in all these grains fall in two groups centred at about 4.30 Ga and 4.20 Ga, similar to the two older groups defined by the six clasts with consistent age distributions. This indicates that although some of the zircon grains are partially disturbed, older ages identified in these grains still define the crystallisation ages of the parent rocks.

Finally three clasts in thin section 14303,52 contain zircon grains that were analysed once (Fig. 6C). Two of these grains show ages similar to the previously defined groups and probably represent the age of crystallisation of the parent rock, while one (grain 8, Table 1) has an intermediate age of about 4.15 Ga and could reflect some degree of resetting of the U–Pb system. It is important to note that 75% of analyses of zircon in the clasts give primary ages of crystallisation of their parent rocks. The range of zircon ages in the mafic and ultramafic rocks from 4.35 to 4.05 Ga is similar to that determined by Meyer et al. (1996) on zircons from granite clasts. In addition, the age distributions appear to be uneven, with three main periods of magmatism at ca. 4.34–4.31, 4.21–4.18 and 4.03–4.00 Ga. There is some

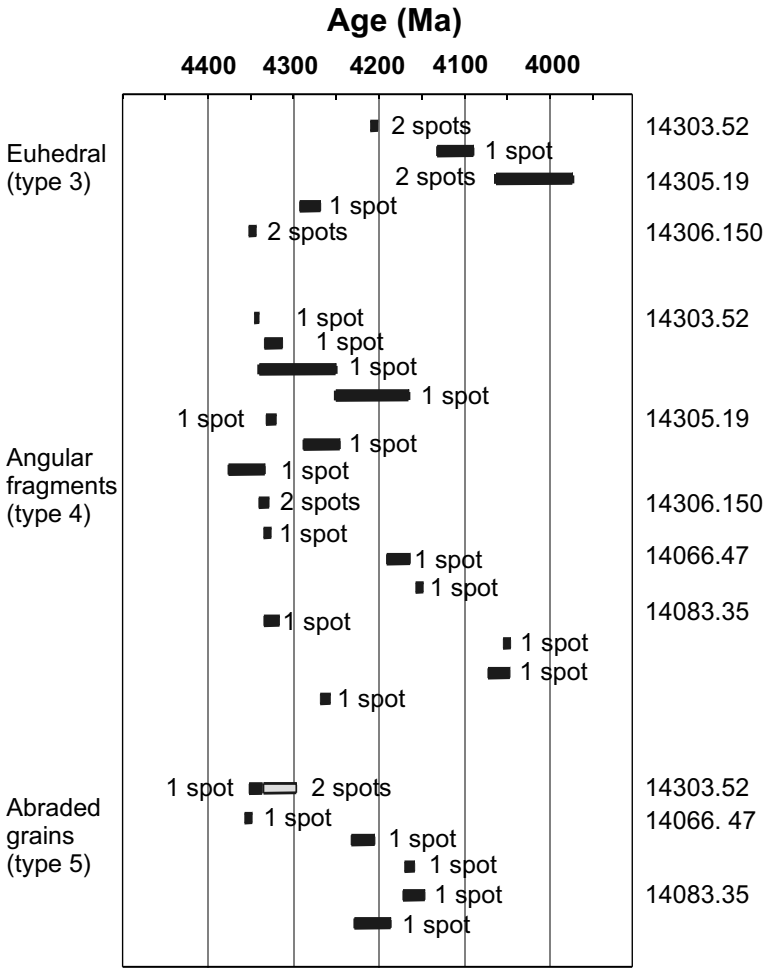

Fig. 7. Distribution of $^{207}Pb/^{206}Pb$ ages of zircon grains from the matrix of Apollo 14 breccias (box lengths are 2-sigma).

suggestion of similar age peaks in the relative probability distribution of zircon ages from granite clasts reported by Meyer et al. (1996).

7. THE AGE DISTRIBUTION OF ZIRCON IN THE MATRICES OF BRECCIAS FROM APOLLO 14

Zircon grains of Types 3, 4, 5 in the breccia matrix cannot be related directly to an igneous parent and could therefore have a different origin and age distribution to that of zircons found as constituents of igneous rock clasts. This could be reflected as a difference in the distributions of zircon ages from mineral clasts and separate matrix zircons. However, comparison of the distribution patterns of the ages of individual zircon grains in the breccia matrices (Fig. 7) with the ages of zircons present in rock clasts (Fig. 6) in Apollo 14 breccias shows that they are similar. Both show peaks, reflecting magmatic activity at about 4.35–4.30 Ga, 4.25–4.20 Ga and about 4.05–4.00 Ga, suggesting that separate zircons and zircons from clasts have a similar magmatic history.

From the morphology of the matrix zircons it could also be possible that the strongly rounded forms (Type 5) present in the breccia matrix had a longer history of transport and abrasion and are older than euhedral grains (Type 3) also present in the matrix. However this is not supported by the results (Fig. 7). Five euhedral zircons (Type 3) from the matrices of Apollo 14 breccias, have ages in the range 4019 ± 14 Ma (sample 14305,19,4-1) to 4352 ± 5 Ma (sample 14306,150,1-1). In comparison, the ages of six type 5 round "abraded" zircons (Table 1) fall in the range 4163 ± 8 Ma (14083,35,4-1) to 4352 ± 3 Ma. (14066,47,3-1). While this small data set is not statistically significant the results indicate that euhedral zircons and round "abraded" zircon grains have broadly similar age distributions, showing that the degree of abrasion is not a significant factor in identifying young grains. The ages of euhedral zircons from the matrices of Apollo 14 breccias are all older than the age of the Imbrium impact defined from Ar–Ar analyses as 3.85 Ga (Stöffler et al., 2006) and from U–Pb zircon analyses as 3909 ± 8 Ma (Gnos et al., 2004).

8. AGE DISTRIBUTIONS OF ZIRCONS FROM INDIVIDUAL BRECCIAS

Although the number of zircons analysed in many individual breccia samples is limited, we have sufficient data in a few cases to give a preliminary impression of the zircon

age distribution for an individual breccia and to test the conclusion of Meyer et al. (1989) that matrix zircons and zircon in rock clasts from the same breccia often show similar wide variation of ages consistent with a wide variety of sources.

8.1. Apollo 14 samples

Zircon age distributions for two breccias from Apollo 14 (14303 and 14321) are shown in Fig. 8.

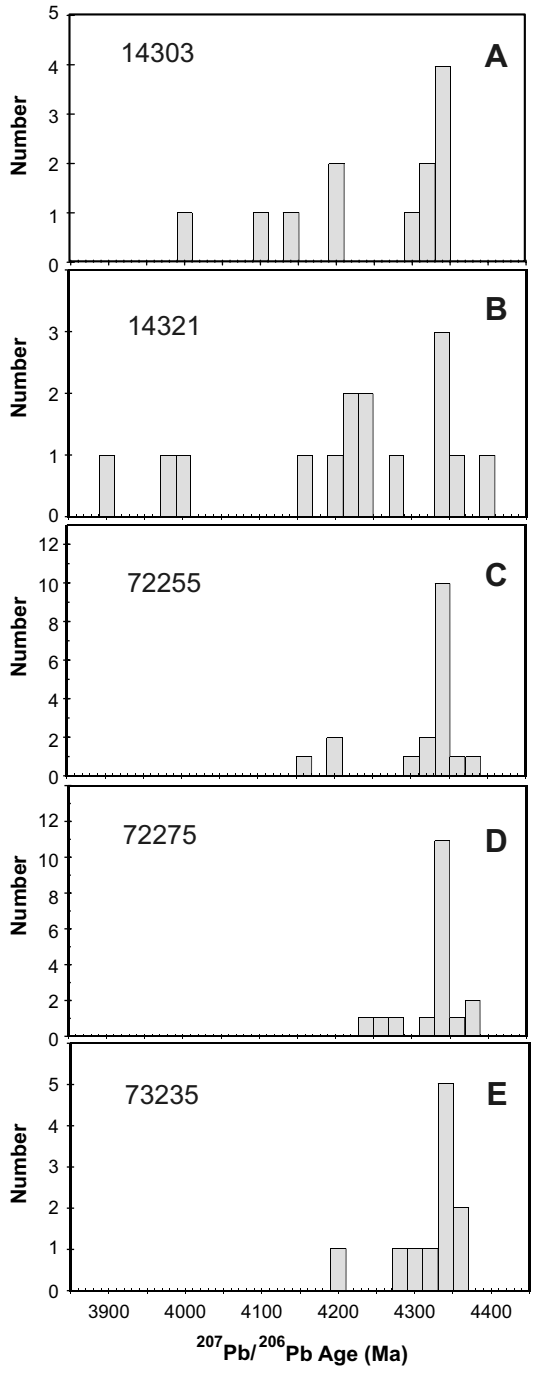

Fig. 8. Histograms showing the distribution of all zircon ages from two Apollo 14 breccia samples (A, and B) and three breccias from Apollo 17 (C–E).

Breccia sample 14303: Thin sections 14303,49 and 14303,52 contain a population of crystal clasts dominated by plagioclase, pyroxene, olivine and a minor opaque minerals. Some norite, pyroxene and olivine rich clasts and older generation breccias are also present in both sections. In addition, thin section 14303,49 contains basaltic clasts with ophitic textures and a single large (10–15 % of the thin section) felsic clast, which was also characterised by Warren et al. (1983) as partially molten "granite". Four zircon grains identified in this clast range in size between about 80 μm and almost 700 μm and appear to be shattered (probably shocked). Six SIMS analyses were made on these four grains (Table 1). Four of the analyses gave ages ranging from 4316 ± 2 to 4346 ± 2 Ma, while additional analyses of two grains are distinctly younger with ages of 4298 ± 4 and 4296 ± 7 Ma. Two SIMS analyses of a single grain from a different thin section of the same clast, presented by Meyer et al. (1996), show intermediate ages of 4314 ± 5 and 4304 ± 4 Ma. Four zircon grains analysed in thin section 14303,52 occur within rock clasts or form composite aggregates with rock forming minerals. Grain 3 is included in a spherical olivine–pyroxene clast about 2 mm in size. One of three analyses of this zircon has a ^{207}Pb/^{206}Pb age of 4313 ± 29 Ma, whereas the other two are younger but similar in age at 4179 ± 56 and 4129 ± 20 Ma. The two different ages probably reflect both original crystallisation of zircon from the melt and resetting of the U–Pb system during an impact. Grain 8 is included in a small (about 200 μm) plagioclase-pyroxene clast and contains numerous inclusions. A single analysis of this grain has a ^{207}Pb/^{206}Pb age of 4150 ± 8 Ma. Grain 1 is almost completely surrounded by several pyroxene grains and has a ^{207}Pb/^{206}Pb age of 4008 ± 8 Ma determined from one analysis. One analysis of grain 4 attached to a plagioclase clast gave a ^{207}Pb/^{206}Pb age of 4340 ± 49 Ma. The remaining seven zircons in the section are located in the breccia matrix. Three analyses on grain 6 show a small spread of ^{207}Pb/^{206}Pb ages between 4343 ± 5 and 4306 ± 7 Ma, whereas two analyses on grain 5 have identical ^{207}Pb/^{206}Pb ages of 4209 ± 4 and 4205 ± 9 Ma. The remaining four grains are about 30–60 μm and allow only one analytical spot to be fitted on their surface. From the histogram plot in Fig. 8A, it is evident that the distribution of the ages covers almost the entire range of ^{207}Pb/^{206}Pb ages of zircons (youngest age ca. 4.00 Ga) from Apollo 14 samples listed on Table 1.

Breccia sample 14321: Two zircon grains were identified inside a single anorthosite clast in thin section 14321,16. Both preserve crystallographic faces. Three analyses of these grains give similar ^{207}Pb/^{206}Pb ages of 4053 ± 11, 4025 ± 42 and 4021 ± 6 Ma, which are interpreted to represent the age of anorthosite formation. An additional fifteen zircons were analysed from the sawdust sample from the breccia (Table 1). The uranium contents of the zircons varied from 7 ppm (grain 2) to 808 ppm (grain 1) indicating a diverse origin for the zircons. Fourteen of the grains were analysed at least twice and the repeat analyses of 13 of these agree to within experimental error. Only grains 8 and 13 showed a significant age discrepancy between duplicate analyses suggesting that the U–Pb systems have been dis-

turbed. Analyses of these grains were omitted from the histogram plot (Fig. 8B). The ages shown on the histogram plot extend over the entire range of ages of ca. 4.36–4.00 Ga shown by all analysed Apollo 14 zircons.

Zircon analyses from breccias 14305, 14306, 14066 and 14083 show similar age patterns to that in 14303 and 14321 but have insufficient analyses to be presented as histograms.

8.2. Apollo 17 samples

Histograms of zircon ages for Apollo 17 breccias 72255, 72575 and 73235 are presented in Fig. 8.

Breccia sample 72255: Eighteen zircon grains ranging in size from about 20 to about 50 μm were separated from sawdust collected during cutting of the sample. Fourteen of these grains are older than 4.30 Ga and only one is significantly younger than 4.20 Ga having $^{207}Pb/^{206}Pb$ age of 4158 ± 5 Ma (Table 2). A histogram of the ages in Fig. 8C shows a strong group of ages at ca 4350 Ma and a lesser group at ca. 4200 Ma.

Breccia sample 72275: Eighteen grains separated from the sawdust of sample 72275 are all older than 4.20 Ga, and only three grains are younger than 4.30 Ga (Table 2). The histogram plot of zircon ages (Fig. 8D) shows a strong peak at 4350 Ma and are all within the restricted range 4220 Ma to 4360 Ma, essentially identical to that observed for zircons from 72255 (Fig. 8D).

Breccia sample 73235: Lithic clasts in the sample include granoblastic feldspathic impactities with a variety of grain sizes, shocked anorthosites, and cataclasized troctolites and norites. Many lithic clasts are strung out as schlieren within the dense matrix. Pidgeon et al. (2007) described a complex fractured zircon in an anorthosite clast from section 73235,82. Three newly investigated sections of this sample contain an additional eleven zircon grains. Five grains were found in the matrix of section 73235,54. Four are angular fragments 25–35 μm in size. Two of these grains have identical $^{207}Pb/^{206}Pb$ ages of 4290 ± 10 and 4287 ± 15 Ma whereas the other two have identical but older $^{207}Pb/^{206}Pb$ ages of 4324 ± 4 and 4332 ± 5 Ma. The remaining grain is also an angular fragment but is about 200 μm in size. Two analyses of this grain are indistinguishable within error at 4344 ± 6 and 4355 ± 5 Ma. Of three zircon grains from the matrix of sample 73235,60, two show clear signs of abrasion, possibly during breccia formation, and have ages in excess of 4.30 Ga. Two ages determined on one of these grains (4305 ± 5 and 4347 ± 8 Ma) are significantly different. The older age is similar to the 4342 ± 5 Ma age obtained for the second grain. The third grain, which has regular crystal faces is about 50 μm in size and also has an age of 4355 ± 6 Ma. The fourth grain found in this section is euhedral and enclosed in a plagioclase grain. Two analyses of this grain gave an age of ca. 4200 Ma. Two zircon grains about 45 μm and about 90 μm in size were found in section 73235,80. Both appear to be abraded. The larger was analysed twice and has ages older than 4.30 Ga that are indistinguishable within error. Two analyses of the smaller grain are different with $^{207}Pb/^{206}Pb$ ages of 4213 ± 14 and 4345 ± 18 Ma. The ages, shown on a histogram plot in Fig. 8E, form a main group from 4280 to 4360 Ma and a minor group at ca. 4200 Ma.

SIMS U–Pb analyses of ages of three zircons from breccia 73215 and two from breccia 73217 (Table 2) fall in the age range 4.35–4.20 Ga. These are in accord with the zircon age distributions of Apollo 17 breccias (Fig. 8C–E) which fall within the restricted range 4.36 Ga to 4.16 Ga. The latter age is from sawdust sample 72255 with an age of 4158 ± 5 Ma. Similar ages in a zircon grain from the sample 76295 have been interpreted as reflecting a partial Pb loss from the rim of this grain (Pidgeon et al., 2006). If the 4158 ± 5 Ma zircon from the sample 72255, is also found to be a result of Pb loss, primary ages of Apollo 17 zircons would all be older than about 4.2 Ga.

9. THE CONSISTENCY OF ZIRCON AGES ACROSS THE TRAVERSED AREAS

The breccias of the Fra Mauro Formation sampled by Apollo 14 have been interpreted to be primary Imbrium ejecta (Wilhelms, 1987; Hiesinger and Head, 2006) or a mixture of dominantly local material intermixed with 15–20% Imbrium ejecta (Morrison and Oberbeck, 1975). The impact melt breccias of Taurus-Littrow valley sampled by Apollo 17 are interpreted as Serenitatis ejecta (Hiesinger and Head, 2006). On the other hand Haskin (1998) and Haskin et al. (1998) proposed that all landing sites have been strongly influenced by material derived from one or few late basins especially Imbrium. The present samples provide an opportunity to investigate the consistency of the zircon age distributions within the traversed areas of the Apollo 14 and 17 landing sites and to answer the question of the independence or otherwise of the two areas in terms of lunar history.

9.1. The Apollo 14 landing site

Samples from Apollo 14 are distributed over a traverse length of about 1.5 km (Fig. 1). They consist of a western group of samples (14303 and 14305) collected 80 m NNW of the landing site, a central group samples (14306 and 14066) collected 230 m and 450 m ESE of the landing site and an eastern-most group (samples 14083 and 14321) collected at station-C1, near the rim of Cone Crater, 1.24 km ENE of the landing site.

The zircon SIMS data, shown in Table 1, are grouped according to location (Fig. 1). The samples are grouped to show up any age variations across the traversed area. However all sample groups show a similar pattern of ages on the histogram plots (Fig. 9), with a spread in zircon ages from ca. 4.37 to ca. 4.00 Ga and apparent age peaks at ca. 4.35 Ga, ca. 4.20 Ga and ca. 4.00 Ga. The absence of any significant variation in the pattern of zircon ages across the Apollo 14 traverse suggests a uniformity of parent rocks and/or a comprehensive mixing of zircons from rocks of a variety of lithologies with a wide age range. Based on this uniformity in age patterns it is valid to prepare a combined Apollo 14 site age distribution, by compounding the ages of 52 grains from all Apollo 14 breccia samples. This age distribution (Fig. 10) shows an almost continuous spread in

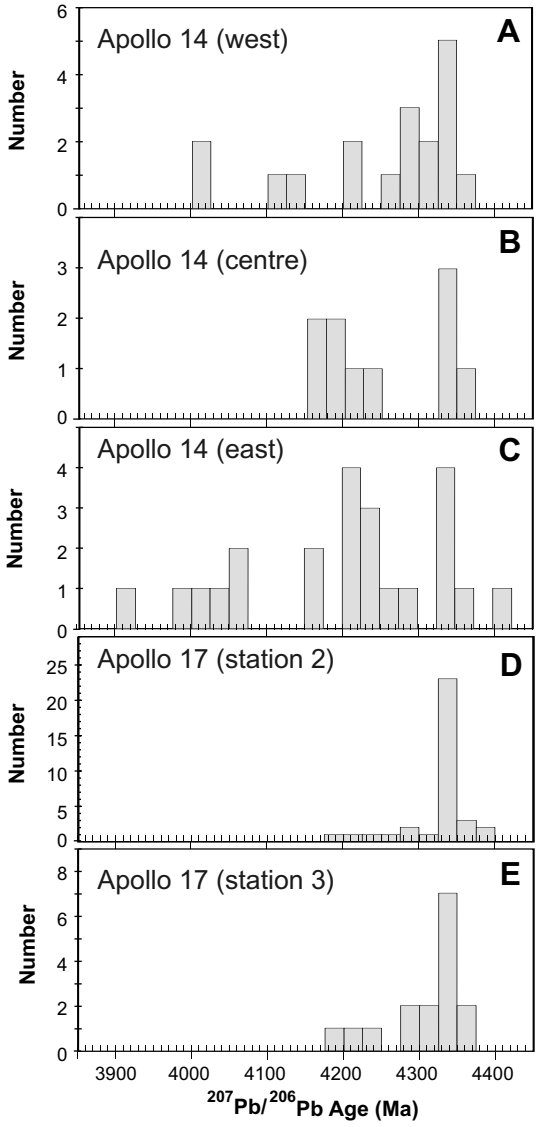

Fig. 9. Histograms showing the areal distribution of zircon ages in breccias from the western (A), central (B) and eastern (C) areas of Apollo 14 and the station 2 (D) and station 3 (E) areas of Apollo 17.

ages from ca. 4.37 Ga to ca. 3.90 Ga. However, the age distribution is not uniform but has definite age peaks at ca 4.35 Ga, ca. 4.20 Ga and ca. 4.00 Ga. The age peaks are followed by deceasing zircon ages and age troughs are evident at ca. 4.25 Ga, 4.10 Ga and 3.92 Ga.

9.2. The Apollo 17 landing site

Breccia samples from the Apollo 17 Taurus-Littrow region are concentrated in the area of the South Massif. Samples 72255 and 72275 are from the different parts of boulder-1 at station-2 about 50 m above the break in slope on the Massif and about 7 km SW of the landing site. The boulder probably came to rest after rolling from the upper portions of the Massif. Samples 73215, 73217 and 73235 were collected at station-3, about 2 km NNE of station-2. The samples are part of the light coloured mantle material from a landslide off the South Massif. At the other end of the traverse sample 76295 was chipped off a large boulder at station-6 about 3 km NNE of the landing site. Tracks made by this boulder indicate that it originated high up on the North Massif.

The Apollo 17 samples cover a traverse distance of approximately 10 km and the two main groups, station-2 (72255 and 72275) and station-3 (73215, 73217 and 73235) are about 3 km apart. Any variation in the age patterns across the traverse should be apparent from the distribution of the two groups. However, the age distributions for the two groups are essentially identical (Fig. 9) indicating a uniformity in the distribution of zircon ages across this 3 km section of the area. The primary ages of two grains from sample 76295 near the North Massif, in the far north east of the traversed area, are in accord with the observed age patterns in the breccia samples (Fig. 9) from the south western, station 3 samples, indicating that the age distribution of zircons in breccias over the 10 km traverse length of the Apollo 17 landing area are broadly similar. Consequently, the area can be represented by a composite age distribution, prepared by compounding the primary ages of 53 zircons from analysed Apollo 17 breccia samples. This distribution (Fig. 10) shows a pattern of ages dominated by a peak at ca 4350 Ma and a possible minor peak at 4200 Ma. No reliable primary zircon ages present in the Apollo 17 samples are younger than ca. 4200 Ma.

10. THE COMBINED ZIRCON AGE DISTRIBUTIONS

10.1. Zircon age profiles

The most striking result of the present study is the difference between the zircon age profiles from the Apollo 14 and Apollo 17 landing sites. Both Apollo 14 and Apollo 17 zircons have essentially identical age patterns in the age range 4.35–4.20 Ga. However, whereas Apollo 14 zircons also have ages in the range 4.20–3.90 Ga, the Apollo 17 samples have no zircons with ages <4.16 Ga and possibly not less than 4.20 Ga. This pattern is reproduced consistently irrespective of whether the full set of analyses representing the landing site is used to construct the age distribution diagram or these analyses are split into the groups according to zircon textural features, or location of sample within the traverse. This remarkable consistency suggests a comprehensive mixing of zircons from a variety of rock types with a wide age range over the traversed areas of the two landing sites. This mixing can be attributed mainly to impacts responsible for the formation of the breccias (Imbrium impact for the Apollo 14 and Serenitatis impact for the Apollo 17 samples). The difference in the age distributions demonstrates the independence of the source rocks between the two landing site areas and also demonstrates that there has been no significant mixing of materials between the two areas.

10.2. Zircon age peaks

Meyer et al. (1996) suggested that zircon forming lunar magmatism was most active prior to 4.30 Ga and was con-

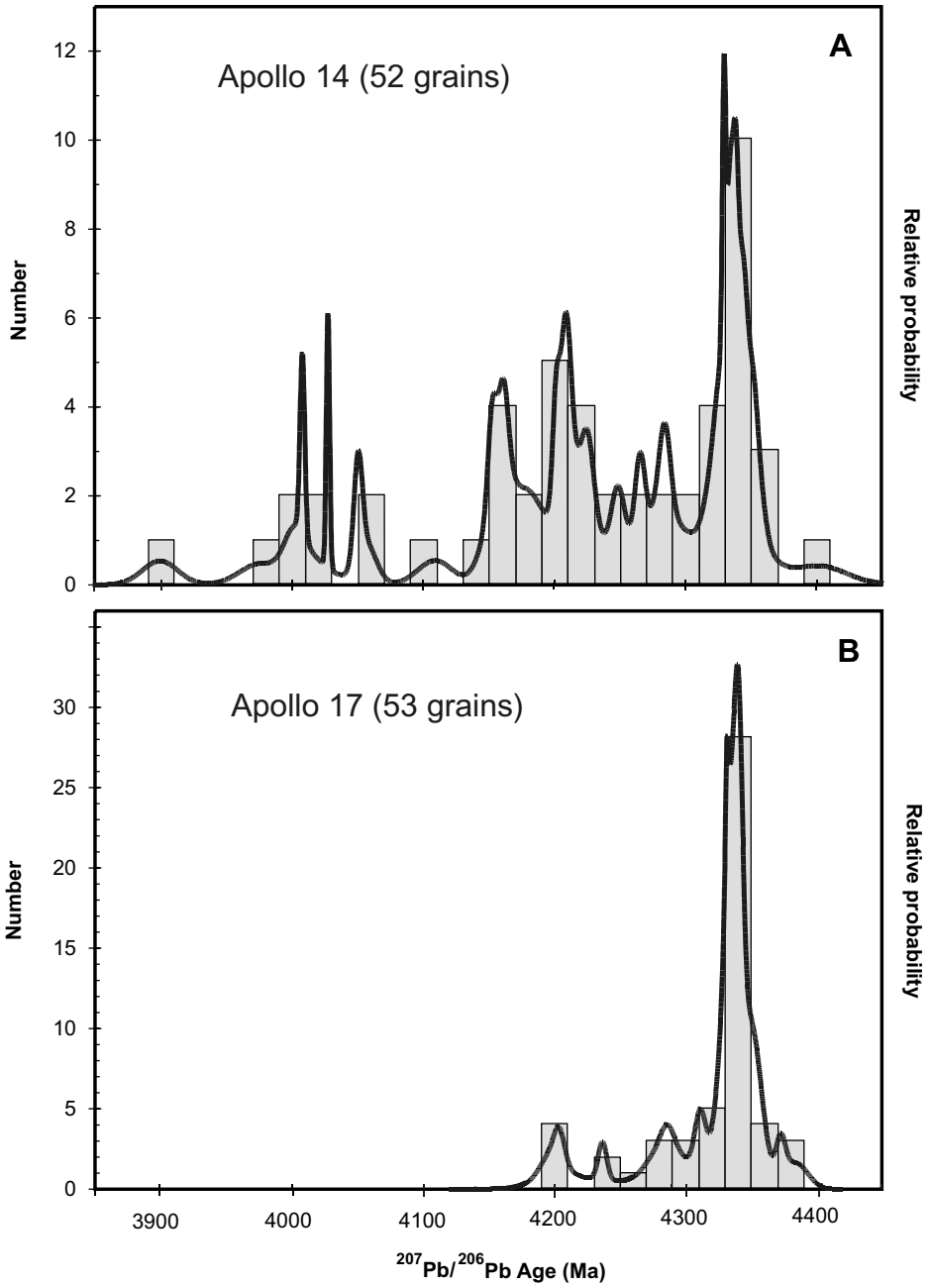

Fig. 10. Combined relative probability plots and histograms of zircon ages from Apollo 14 (A) and Apollo 17 (B) breccias.

tinuous until at least 3.88 Ga. However, results obtained from the present study show that this continuum of ages is not smooth but consists of a number of distinctive age peaks with surrounding troughs (Fig. 10). The age peaks are not sharply defined but occur as a distribution of decreasing ages around a central peak (Fig. 10). In the Apollo 14 zircon age distribution peaks of KREEP magmatism are recorded at ca. 4.35 Ga, ca. 4.20 Ga and possibly ca 4.00 Ga and there are age troughs at ca. 4.25 Ga and ca. 4.10 Ga. Only a few ages are younger than 4.00 Ga. It is notable that only one zircon (14321–24) has an age of ca. 3.85 Ga, similar to the age of 3.85 ± 0.02 Ga (Stöffler et al., 2006) or 3909 ± 13 Ma (Gnos et al., 2004) determined for the impact and formation of the Imbrium basin. The Apollo 17 distribution also shows peaks at 4.35 Ga and 4.20 Ga and a trough at 4.25 Ga, but has no ages younger than ca. 4.20 Ga. The age peaks described above are also detected in the distribution of lunar granophyric zircon ages presented by Meyer et al. (1996). Zircon ages are generally interpreted as dating magmatic events (e.g. Meyer et al., 1996) and we interpret the zircon age peaks as marking periodic episodes of KREEP magmatism where each magmatic episode involved a spectrum of lithologies of KREEPy mafic–ultramafic and granophyric rocks.

11. DYNAMIC MODEL OF KREEP EVOLUTION

11.1. Contraction of KREEP magmatic activity over time

The discrepancy in the record of zircon ages between the Apollo 14 and 17 regions records a profound areal change of lunar magmatic activity with time.

These observations can be related to the discovery by the Lunar Prospector (Lawrence et al., 1998, 2000) that the surface abundances of incompatible elements, including Th and probably other characteristic KREEP elements, are highly concentrated in a single region that encompasses Oceanus Procellarum, Mare Imbrium and the adjoining mare and highlands and is referred to as the Procellarum KREEP terrane (Haskin et al., 2000; Jolliff et al., 2000; Wieczorek and Phillips, 2000). The Imbrium impact, represented by the Apollo 14 samples is located near the centre of the Procellarum KREEP terrane, whereas the Serenitatis crater represented by Apollo 17 samples is situated at the edge of the high Th region (Jolliff et al., 2000).

The zircon age distributions suggest that the generation of KREEP magma in the region of the Apollo 17 site (Serenitatis impact crater area) ceased at about 4.20 Ga, whereas it continued for another 200–300 m.y. in the terrain that was the source of material sampled by the Apollo 14 mission (Imbrium impact crater area). Previous zircon age determinations on Apollo 17 and Apollo 14 zircons are compatible with this conclusion. Meyer et al. (1996) reported zircon ages of granophyric clasts from Apollo 14 rocks down to ca. 3.90 Ga. The few zircons from Apollo 17 samples previously measured all have ages in excess of 4.20 Ga (Compston et al., 1984b; Meyer et al., 1985; Pidgeon et al., 2007).

Thermal modelling that assumes high heat production in this area, associated with the strong enrichment of KREEP in radioactive elements, suggests that a molten KREEP rich source existed in this region for an extended period of time and supported prolonged magmatic activity (e.g. Wieczorek and Phillips, 2000). If this view is correct, the lateral distribution of zircon ages may reflect shrinking of this source between 4.38 and 3.90 Ga towards the middle of the Procellarum KREEP terrane. Between 4.38 and 4.20 Ga the region under the lunar crust where a semi-molten KREEP source was present extended beyond the area highlighted by the Th anomaly and included the Apollo 17 location. However, by 4.20 Ga this region was laterally reduced to the central part of the Procellarum KREEP terrane and excluded the area of the Serenitatis impact, as indicated by the Apollo 17 zircon age record.

11.2. Episodes of lunar magmatism

The history of KREEP magmatism from ca. 4.37 Ga to ca. 3.90 Ga is dominated by pulses of KREEPy magma generation and emplacement at ca 4.35 Ga, ca. 4.20 Ga and possibly ca. 4.00 Ga. The first major episode of magmatic activity occurred in the time interval 4.37–4.33 Ga with a strong peak at ca. 4.35 Ga. This represents the first generation and preservation of KREEPy rocks on the Moon and is the largest KREEP-magma forming event. This event was widespread as evidenced by the presence of an identical age peak in zircon age distributions for samples from Apollo 14 and Apollo 17.

Meyer et al. (1985) reported the ages of four felsite zircons to be as old as 4.35 Ga and suggested that this is the apparent closure age of the lunar crust, indicating that the original magma ocean had completely solidified by 4.35 Ga. This is compatible with the recent report of Touboul et al. (2007) of W isotope data on metals from low and high-Ti mare basalts. They suggested that only a few samples preserve small ^{182}W anomalies, which is consistent with a prolonged crystallisation of the LMO, and is compatible with the ^{146}Sm–^{142}Nd model age of the LMO of about 215 m.y. after the formation of the Solar System (Nyquist et al., 1995) which is also in accord with the oldest zircon ages.

The earliest lunar crust is thought to have formed by the accumulation of plagioclase (ferroan anorthosites) during cooling and crystallisation of the primitive magma ocean (Shearer et al., 2006). Attempts to date ferroan anorthosites by Ar–Ar and Rb–Sr proved to be difficult, but Sm–Nd internal isochron ages of 4.51–4.44 Ga have been determined for FAN by Carlson and Lugmair (1988) and Alibert et al. (1994) although Borg et al. (1999) obtained a younger ferroan anorthosite Sm–Nd age of 4.36 ± 0.03 Ga. The inconsistencies in the Sm–Nd data need to be resolved but on face value it appears that the oldest 4.37–4.35 Ga, group of zircon ages are similar or possibly slightly younger than the age of the ferroan anorthosites.

A second event at ca. 4.2 Ga activated a new pulse of KREEP magmatism from a now significantly contracted primary reservoir of KREEP melt. As a result of this contraction the extent of KREEP magma generation was much smaller in the area represented by the Apollo 17 samples, whereas in the area represented by Apollo 14 samples it was similar in magnitude to the 4350 Ma KREEP magma generation event. Recognition of a second ca 4200 Ma magmatic episode raises significant questions about the processes of lunar magmatism, including processes responsible for the first 4350 Ma magmatic episode. A third event at 4000 Ma resulted in a small magmatic pulse in the Imbrium impact area. The relatively small spike in the age distribution suggests that, at this time, the region represented by the Apollo 14 site was itself on the outer margin of the continually contracting KREEP reservoir.

This episode appears to precede the final extrusion of KREEP magma as evidenced by fine-grained fragments of pristine KREEP basalt (e.g. 15382, 15386). This extrusion has been very well dated by both Rb–Sr (Nyquist et al., 1975) and Sm–Nd (Carlson and Lugmair, 1979) at 3.9 Ga, and is thought to be contemporaneous with and possibly triggered by the Imbrium impact (Ryder, 1994). This episode may also be recorded by the age of zircons in lunar meteorite SAU169 (Gnos et al., 2004).

The presence of pulses of activity in the history of lunar KREEP magma emplacement has not been previously considered in models of lunar evolution. A major question concerns the nature of the triggering mechanism. One possibility is that large impacts activated the primary KREEP reservoir resulting in spikes of KREEP magmatism. An exponentially decreasing flux of bolides impacting

the early Moon could be punctuated by a few very large impacts at ca. 4.35, 4.20 Ga and 3.9 Ga which have the potential to trigger magmatic activity. The striking observation that essentially all the KREEPy rocks excavated by the last major impact events at ca. 3.9 Ga (Imbrium, Serenitatis) are significantly older than these impacts could be taken as evidence that there was no magmatism associated with proposed lunar cataclysm at ca. 3.9 Ga. However, 3.9 Ga magma generation may have occurred and be present sub-surface in the vicinity of Imbrium basin in the Procellarum KREEP terrane.

The periodic production of KREEP-rich rocks, and the contraction of the primary KREEP reservoir could also be explained by endogenic processes, and while the nature of the actual mechanisms may not be clear, they are evidently linked to the thermal history of the Moon. Recent models that attempt to explain the observed asymmetry in the concentration of Th, mare volcanism, the thickness of lunar crust etc have been summarised by Shearer et al. (2006). One of these models (Wieczorek and Phillips, 2000) describes the thermal evolution of the Procellarum KREEP terrane and suggests that the accumulation of KREEP material rich in radioactive elements would result in the long term melting of the KREEP source as well as gradual heating of the underlying mantle and that Mare volcanism would span most of the Moon's history. This model does not account for the observed zircon age distribution patterns, which suggest periodic pulses of KREEP magmatic activity in the area during the first 500 Ma. However, following this model, a possible explanation for our results envisages a build-up of radioactive heat in the KREEP reservoir until the buoyancy of the KREEP melt exceeded the strength of the overlying rocks resulting in a sudden transfer of KREEP magma and heat into the crust. The observed pattern of an initial KREEP magma pulse followed by declining magmatism could be explained by proposing that KREEP magmatism represented the transfer of a large body of KREEP magma from the deep reservoir to an independent, intermediate reservoir in the crust where the gradual decline in magmatism reflected the cooling of this reservoir. At the same time the deep seated reservoir gradually reheated through U, Th and K decay, until the process was repeated and a second pulse of magmatism results in the transfer of a further generation of KREEP magma into the crust. Whereas this model is consistent with our observations other possible models of the thermal history of the Procellarum KREEP Terrane could quite well fit the zircon data. However, these will need to account for the peaks in KREEP magmatic activity at ca. 4.35 Ga, ca. 4.20 Ga and ca. 4.00 Ga the paucity of ca. 3.85 Ga zircons (and hence KREEP rocks of this age) in the 3850 ± 20 Ma Imbrium impact ejecta (Stöffler et al., 2006) and the lack of any zircons (KREEP rocks) younger than 4.20 Ga in ejecta of the 3893 ± 9 Ma (Dalrymple and Ryder, 1996) Serenitatis event.

12. SUMMARY AND CONCLUSIONS

Zircons present in igneous clasts and as loose grains in lunar breccias crystallised from older parent rocks and have largely survived heating and abrasion associated with impact and breccia formation. Our results confirm previous conclusions that individual lithologies such as granite and norite have a wide range of crystallisation ages between 4.38 and 3.90 Ga indicating that lunar processes have generated multiple magmatic cycles forming a similar range of magmatic products, and that these have been comprehensively mixed on the scale of individual breccias. The age distribution of individual zircons from the breccia matrices is not significantly different from the age distribution of zircons from igneous clasts in any breccia, suggesting the two occurrences of zircons are from similar sources. The possibility that rounded zircon grains in a breccia matrix have experienced a greater abrasion history and are older than euhedral zircons also present in the breccia matrices is not supported by the U–Pb ages which are not significantly different between the two zircon types showing that the degree of abrasion is not a reliable guide to relative age of the grains.

Our SIMS results show that ages of zircons from breccias from Apollo 14 spread from ca. 4.38 Ga to ca. 3.90 Ga, whereas ages of zircons from Apollo 17 breccias vary from ca. 4.35 Ga to ca. 4.20 Ga. Within each Apollo landing site the zircon age patterns show no observed variation from one end of the traversed area to the other. These zircon U–Pb ages demonstrate a profound difference in the timing of KREEP magmatism between the Apollo 14 and Apollo 17 landing sites. Whereas a record of igneous activity from 4.38 to 3.90 Ga is preserved in zircons from breccias from the Apollo 14 site, the record of KREEP magmatism in breccias from the Apollo 17 site extends only from 4.35 to 4.20 Ga. No primary zircon ages were found in the Apollo 17 breccias younger than 4.20 Ga. On this evidence there has been no addition or mixing of 3.85 Ga Imbrium ejecta into the rocks of the Taurus-Littrow Valley interpreted to be dominated by Serenitatis ejecta. In addition our SIMS U–Pb results show that the KREEP magmatic record is irregular, consisting of two or three major magmatic episodes at 4.35 Ga, 4.2 Ga and possibly 4.0 Ga, followed by declining magmatic activity. These observations provide a new foundation for understanding the dynamics of lunar magmatism. In explanation we propose that KREEP magmatism was generated from a deep seated source that was not static but contracted over time from unknown initial margins towards the centre of the Procellarum KREEP terrane. Pulses of magmatic emplacement into the overlying crust were triggered by large meteorite impacts or occurred in response to the periodic release of heat accumulated within the KREEP reservoir as a result of radioactive decay. Further research on complex zircon grains and additional analyses of zircons from breccias from other Apollo sites will be needed to resolve these issues.

ACKNOWLEDGMENTS

In particular we thank the astronauts of Apollo 14 and Apollo 17 for risking their lives to collect the samples. This paper benefited from helpful comments of Steve Reddy. Very constructive comments of Bradley Jolliff, two anonymous reviewers, as well as suggestions of associate editor of Geochimica et Cosmochimica. Acta

Randy Korotev are greatly appreciated for their thoroughness and high content of useful information. The NordSIM facility, (Swedish Museum of Natural History) is supported by the research councils in Denmark, Finland, Norway and Sweden together with the Swedish Museum of Natural History. This is the NordSIM publication #197. The SHRIMP laboratory at Curtin is part of the John deLaeter Centre for Mass Spectrometry supported by a grant from the government of Western Australia.

REFERENCES

Alibert C., Norman M. D. and McCulloch M. T. (1994) An ancient age for a ferroan anorthosite clast from lunar breccia 67016. *Geochim. Cosmochim. Acta* **58**, 2921–2926.

Borg L. E., Norman M., Nyquist L., Bogard D., Snyder G., Taylor L. and Lindstrom M. (1999) Isotopic studies of ferroan anorthosite 62236: A younger lunar crustal rock from a light rare-earth-element-depleted source. *Geochim. Cosmochim. Acta* **63**, 2679–2691.

Carlson R. W. and Lugmair G. W. (1979) Sm–Nd constraints on early lunar differentiation and the evolution of KREEP. *Earth Planet. Sci. Lett.* **45**, 123–132.

Carlson R. W. and Lugmair G. W. (1988) The age of ferroan anorthosite 60025: Oldest crust on a young moon? *Earth Planet. Sci. Lett.* **90**, 119–130.

Clement S. W. J. and Compston W. (1989) SIMS at high sensitivity and high mass resolution. In *Proc. 7th Intl. Conf. Secondary Ion Mass Spectrometery*. Wiley.

Compston W., Williams I. S. and Meyer C. (1984a) U–Pb geochronology of zircons from Lunar Breccia 73217 using a sensitive high mass-resolution ion microprobe. In *Proc. Lunar Planet. Sci. Conf. 14th*, *J. Geophys. Res.* **89,** B525–B534.

Compston W., Williams I. S. and Meyer C. (1984b) Age and chemistry of zircon from late-stage differentiates. *Lunar Planet. Sci. (abs)* **15**, 182–184.

Compston W., Williams I. S. and Meyer C. (1991) Initial Pb isotopic compositions of lunar granites as determined by ion microprobe. In *Stable Isotope Geochemistry: A Tribute to Samual Epstein*. Geochemical Society Spec. Pub. #3, pp. 473–486.

Dalrymple G. B. and Ryder G. (1996) Argon-40/argon-39 age spectra of Apollo 17 highlands breccia samples by laser step heating and the age of the Serenitatis basin. *J. Geophys. Res.* **101**, 26069–26084.

Dickinson J. E. and Hess P. C. (1982) Zircon saturation in lunar basalts and granites. *Earth Planet. Sci. Lett.* **57**, 336–344.

Gale N. H. (1972) Uranium–lead systematics in lunar basalts. *Earth Planet. Sci. Lett.* **17**, 65–78.

Gnos E., Hofmann B. A., Al-Katgiri A., Lorenzetti S., Eugster O., Whitehouse M. J., Villa I. M. and Jull A. J. T., et al. (2004) Pinpointing the source of a lunar meteorite: implications for the evolution of the Moon. *Science* **305**, 657–659 .

Haskin L. A. (1998) The Imbrium impact event and the thorium distribution at the lunar highland surface. *J. Geophys. Res.* **103**, 1679–1689.

Haskin L. A., Korotev R. L., Rockow K. M. and Jolliff B. L. (1998) The case for an Imbrium origin of the Apollo thorium-rich impact-melt breccias. *Meteoritics Planet. Sci.* **33**, 959–975.

Haskin L. A., Gillis J. J., Korotev R. L. and Jolliff B. L. (2000) The materials of the lunar Procellarum KREEP terrane: a systesis of data from geomorphological mapping, remote sensing and sample analysis. *J. Geophys. Res.* **105**, 20403–20415.

Hiesinger H. and Head J. W. (2006) New views of lunar geoscience: an introduction and overview. In *New Views of the Moon. Rev. Mineral. Geochem.*, vol. 60, pp. 1–81. New Views of the Moon. Rev. Mineral. Geochem.. Mineralogica Society of America (Chapter 1).

James O. B. (1980) Rocks of the early lunar crust. In *Proc. Lunar Planet. Sci. Conf. 11th*, pp. 365–393.

Jolliff B. L., Gillis J. J., Haskin L., Korotev R. L. and Wieczorek M. A. (2000) Major lunar crustal terranes: surface expressions and crust-mantle origins. *J. Geophys. Res.* **105**, 4197–4216.

Kennedy A. K. and de Laeter J. R. (1994) The performance characteristics of the WA SHRIMP II ion microprobe. In *8th Int. Conf. on Geochronology, Cosmochronology and Isotope Geology*, Berkeley, U.S. Geol. Surv. Circ. 1107, p. 166.

Lawrence D. J., Feldman W. C., Barraclough B. L., Binder A. B., Elphic R. C., Maurice S. and Thomsen D. R. (1998) Global elemental maps of the Moon: the Lunar Prospector gamma-ray spectrometer. *Science* **281**, 1484–1489.

Lawrence D. J., Feldman W. C., Barraclough B. L., Binder A. B., Elphic R. C., Maurice S., Miller M. C. and Prettyman T. H. (2000) Thorium abundances on the lunar surface. *J. Geophys. Res.* **105**, 20307–20331.

Ludwig K. (2001a) *Users manual for Squid1.02*. Berkeley Geochronology Center. Special Publication 1a, 19pp.

Ludwig K. (2001b) *Users manual for Isoplot/Ex rev. 2.49*. Berkeley Geochronology Center. Special Publication 2, 55pp.

Meyer C. (1977) Petrology, mineralogy and chemistry of KREEP basalt. *Phys. Chem. Earth* **10**, 239–260.

Meyer C. (1994) *Catalog of Apollo 17 Rocks: Volume 4*. Curator's Office JSC 26088, p. 644.

Meyer C., Brett R., Hubbard N. J., Morrison D., McKay D., Aitken F. K., Takeda H. and Schonfeld E. (1971) Mineralogy, chemistry, and origin of the KREEP component in soil samples from the Ocean of Storms. In *Proc. 2nd Lunar Sci. Conf.*, pp. 393–411.

Meyer C., Compston W. and Williams I. S. (1985) Lunar zircon and the closure age of the lunar crust. *Lunar Planet. Sci. (abs)* **XVI**, 557–558.

Meyer C., Williams I. S. and Compston W. (1989) $^{207}Pb/^{206}Pb$ ages of zircon-containing rock fragments indicate continuous magmatism in the lunar crust from 4350–3900 million years. *Lunar Planet. Sci. (abs)* **XX**, 691–692, LPI.

Meyer C., Williams I. S. and Compston W. (1996) Uranium–lead ages for lunar zircons: evidence for a prolonged period of granophyre formation from 4.32 to 3.88 Ga. *Meteoritics Planet. Sci.* **31**, 370–387.

Morrison R. H. and Oberbeck V. R. (1975) Geomorphology of crater and basin deposits–emplacement of the Fra Mauro formation. In *Proc. 6th Lunar Sci. Conf.*, pp. 2503–2530.

Nyquist L. E., Bansal B. M. and Wiesmann H. (1975) Rb–Sr ages and initial 87Sr/86Sr for Apollo17 basalts and KREEP basalt 15386. In *Proc. 6th Lunar Sci. Conf.*, pp. 1445–1465.

Nyquist L. E. and Shih C. -Y. (1992) The isotopic record of lunar volcanism. *Geochim. Cosmochim. Acta* **56**, 2213–2234.

Nyquist L. E., Wiesmann H., Bansal B., Shih C. -Y., Keith J. E. and Harper C. L. (1995) ^{146}Sm–^{142}Nd formation interval for the lunar mantle. *Geochim. Cosmochim. Acta* **59**, 2817–2837.

Pidgeon R. T., Furfaro D., Kennedy A. K., Nemchin A. A. and van Bronswjk W. (1994) Calibration of zircon standards for the Curtin SHRIMP, In *8th Int. Conf. on Geochronology, Cosmochronology and Isotope Geology*, Berkeley, U.S. Geol. Surv. Circ. 1107, p. 251.

Pidgeon R. T., Nemchin A. A. and Meyer C. (2006) Complex histories of two lunar zircons as evidenced by their internal structures and U–Pb Ages (abs), *37th Annual Lunar and Planetary Science Conference*, League City, Texas. #1548 (abstr.).

Pidgeon R. T., Nemchin A. A., van Bronswijk W., Geisler T., Meyer C., Compston W. and Williams I. (2007) Complex

history of a zircon aggregate from lunar breccia 73235. *Geochim. Cosmochim. Acta* **71**, 1370–1381.

Ryder G. (1993) *Catalog of Apollo 17 rocks: Stations 2 and 3*. Curators Office JSC #26088.

Ryder G. (1994) Coincidence in time of the Imbrium basin impact and Apollo 15 KREEP volcanic flows: the case for impact-induced volcanism. In *Large Meteorite Impacts and Planetary Evolution* (eds. B. O. Dressler, R. A. F. Grieve and V. L. Sharpton), Geological Society of America Special Paper 293, pp. 11–18.

Shearer C. K., Hess P. C., Wieczorek M. A., Pritchard M. E., Parmentier E. M., Borg L. E., Longhi J., Elkins-Tanton L. T., Neal C. R., Antonenko I., Canup R. M., Halliday A. N., Grove T. L., Hager B. H., Lee D. -C. and Wiechert U. (2006) Thermal and Magmatic Evolution of the Moon. In *New Views of the Moon. Rev. Mineral. Geochem.* Mineralogica Society of America, vol. 60, pp. 365–518 (Chapter 4).

Simonds C. H., Phinney W. C. and Warner J. L. (1974) Petrography and classification of Apollo 17 non-mare rocks with emphasis on samples from the Station 6 boulder. In *Proc. Lunar Sci. Conf. 5th*, pp. 337–353.

Simonds C. H., Phinney W. C., Warner J. L., McGee P. E., Geeslin J., Brown R. W. and Rhodes M. J. (1977) Apollo 14 revisited, or breccias aren't so bad after all. In *Proc. Lunar Sci. Conf. 8th*, pp. 1869–1893.

Smith J. M., Meyer C., Compston W. and Williams I. S. (1986) 73235,82 (pomegranate): an assemblage of lunar zircon with unique overgrowth (abs). *Lunar Planet. Sci.* **XVII**, 805–806, LPI.

Snyder G. A., Borg L. E., Nyquist L. E. and Taylor L. A. (2000) Chronology and isotopic constraints on lunar evolution. In *Origin of the Earth and Moon* (eds. R. Canup and K. Righter). U. Arizona Press, pp. 361–396 .

Stacey J. S. and Kramers J. D. (1975) Approximation of terrestrial lead isotope evolution by a two-stage model. *Earth Planet. Sci. Lett.* **26**, 207–221.

Stöffler D., Ryder G., Ivanov B. A., Artemieva N. A., Cintala M. J. and Grieve R. A. F. (2006) Cratering history and lunar chronology. In *New Views of the Moon. Rev. Mineral. Geochem*, vol. 60, pp. 519–596. New Views of the Moon. Rev. Mineral. Geochem. Mineralogica Society of America (Chapter 5).

Stöffler D., Knoll D. H. and Maerz U. (1979). Terrestrial and lunar impact breccias and the classification of lunar highland rocks. In *Proc. 10th Lunar Planet. Sci. Conf.*, pp. 639–675.

Tera F. and Wasserburg G. J. (1972) U–Th–Pb systematics in three Apollo 14 basalts and the problem of initial Pb in lunar rocks. *Earth Planet. Sci. Lett.* **14**, 281–304.

Touboul M., Kleine T., Bourdon B. and Palme H. (2007). The duration of magma ocean crystallization on the Moon—evidence from new W isotope data for metals from high-Ti and low-Ti mare basalts (abs), *38th Annual Lunar and Planetary Science Conference*, League City, Texas. #2385 (abstr.).

Warren P. H., Taylor G. J., Keil K., Shirley D. N. and Wasson J. T. (1983) Petrology and chemistry of two large granite clasts from the Moon. *Earth Planet. Sci. Lett.* **64**, 175–185.

Whitehouse M. J., Kamber B. S. and Moorbath S. (1999) Age significance of U–Th–Pb zircon data from early Archaean rocks of west Greenland—a reassessment based on combined ion-microprobe and imaging studies. *Chem. Geol.* **160**, 201–224.

Whitehouse M. J. and Kamber B. S. (2005) Assigning dates to thin gneissic veins in high-grade metamorphic terranes: a cautionary tale from Akilia, Southwest Greenland. *J. Petrol.* **46**, 291–318.

Wieczorek M. A. and Phillips R. J. (2000) The Procellarum KREEP Terrane: implications for mare volcanism and lunar evolution. *J. Geophys. Res.* **105**, 20417–20430.

Wiedenbeck M., Hanchar J., Pec W. H k., Sylvester P., Valley J., Whitehouse M., Kronz A., Morishita Y. and Nasdala L., et al. (2004) Further characterization of the 91500 zircon crystal. *Geostandards Geoanal. Res.* **28**, 9–39.

Wilhelms D. E. (1987) *The Geologic History of the Moon*. US Geological Survey Spec. Pap. 1348.

Associate editor: Randy L. Korotev